國立臺灣大學理學院物理研究所
碩士論文
Department of Physics
College of Science
National Taiwan University
Master Thesis

GOODS 天區次毫米波星系的聚集
Angular Clustering of Submillimeter Galaxies in GOODS Fields

鄭偉良
Wei-Leong Tee

指導教授：闕志鴻教授 (國立臺灣大學)
Advisor: Tzi-Hong Chiueh, Professor (NTU)
共同指導教授：王為豪副研究員 (中央研究院天文及天文物理研究所)
Co-Advisor: Wei-Hao Wang, Associate Research Fellow (ASIAA)

中華民國 107 年 1 月
January, 2018

doi:10.6342/NTU201800137

doi:10.6342/NTU201800137

國立臺灣大學碩士學位論文
口試委員會審定書

GOODS 天區次毫米波星系的聚集
Angular Clustering of Submillimeter Galaxies in GOODS Fields

本論文係鄭偉良君 (R04222026) 在國立臺灣大學物理研究所完成之碩士學位論文，於民國 107 年 1 月 4 日承下列考試委員審查通過及口試及格，特此證明

口試委員：

闕志鴻 （簽名）
（指導教授）

[illegible]

王為豪

doi:10.6342/NTU201800137

doi:10.6342/NTU201800137

誌謝

首先要感謝偉大的老闆們，王為豪副研究員和闕志鴻教授沒有放棄我。王為豪副研究員是一位非常有耐心且善解人意的指導者，不會讓學生感到壓迫，不吝於分享研究經驗，同時還能對研究給予極具建設性的看法和意見；闕志鴻教授待學生寬厚，富有同理心並願意努力為學生爭取權益，使學生能專心致志於研究上。我也要感謝口試委員們，林彥廷副研究員和林俐暉副研究員對這項研究所提供的幫助以及所面對的問題，使這項工作能夠更加完善。我也很感激早年平下博之研究員所給予的中研院暑期研究計畫的工作機會，讓我堅定了想要從事天文研究的想法。我也要感謝在碩士研究期間幫助過我的朋友、同伴、學長姐，有林征發（Bobby）、羅文斌（Vincent）、林聖傑、侯冠州、邱奕儂、胡耀傑（Jerry）以及天文數學館 R922 的室友們。與他們的學術討論促成了這篇工作的正確性，但我更珍惜與大家一起在荊棘滿佈的研究路上攜手前進的時光，當中的血淚交織、燒肝搞笑都是一生無法抹滅的回憶。

一路走來的研究路坎坷不斷、跌宕起伏，經歷多次的低潮後，終於抵達現在這一步。我非常感激我家人對我所做決定的支持，是因為有他們作為我的後盾我才能義無反顧地進行我想要的研究。我最後要感謝的是 Lia，陪伴我走過我對人生的迷惘時候，也不吝於與我分享她的生活，是她的仁慈和寬容救贖了我，讓我有勇氣向前踏穩自己的步伐，去尋找我人生的下一個里程碑。

doi:10.6342/NTU201800137

doi:10.6342/NTU201800137

Acknowledgements

First and foremost, I would like to thank my advisors Dr. Wei-Hao Wang and Prof. Tzi-Hong Chiueh for their patience and support throughout years in graduate school. I also wish to acknowledge other members in my thesis committee, Dr. Yen-Ting Lin and Dr. Li-Hwai Lin, who provided extremely helpful information that contributed to the completion of this thesis. Valuable contributions to this work have also been brought by helpful discussions with Chen-Fatt Lim (Bobby), Wen-Ping Lo (Vincent), Sheng-Chieh Lin, Kuan-Chou Hou and I-Non Chiu during the course of writing this thesis, and it would not have been possible without their help and support. I also want to thank Dr. Hiroyuki Hirashita, who not only inspired me a lot but also gave me my first opportunity to do research as an undergraduate in the ASIAA Summer Student Program.

I would also like to thank my family for their love and support, in particular my parents who have never urged me to leave the academic field earlier, and always support me for any decision I made. I want to thank my friends and office-mates in R922 of Astronomy-Mathematics Building in NTU throughout the years, for providing mental support as well as welcome distractions during my time there, especially Yao-Chieh Hu (Jerry) companionship and care. Finally I would like to thank Lia, who have always accompanied and supported me, and helped me go through all those struggling moments.

doi:10.6342/NTU201800137

doi:10.6342/NTU201800137

摘要

次毫米波星系為一群於紅外波段非常明亮的星系。因為大氣層吸收帶影響，地面能觀測的窗口在遠紅外波段部分為次毫米波段 ($10^{-6} - 10^{-3}$ m)，主要受到水氣吸收影響。星系演化圖像中，恆星形成過程會伴隨劇烈的紅外波段輻射，故次毫米波星系是瞭解星系演化極為重要的一環。我們使用來自 GOODS 天區 SCUBA-2 次毫米波星系的觀測數據，結合使用 K_s 紅外波段非活躍星系的數據，對兩者做相關性研究，由此推導出星系的空間聚集半徑 r_0 及星系可能存在的暗物質暈 M_halo 大小。本研究發現次毫米波星系的聚集強度比文獻所提及的較低。

doi:10.6342/NTU201800137

doi:10.6342/NTU201800137

Abstract

Submillimeter galaxies (SMGs) are high-redshift galaxies ($z = 1 - 4$) with very bright flux densities in the submillimeter waveband. To study their nature and their role in the galaxies evolution history, we present an angular clustering measurement of SMGs in the GOODS-North and GOODS-South. We make a 2.0 mJy and 0.5 mJy cut on 850 μm flux density and noise. The total available SMG sources are 141, with 75 in North and 66 in South. Due to the large uncertainties induced from small size target autocorrelation, we conduct a cross-correlation between target and tracer with larger size to effectively reduce the uncertainties. We use ~ 2500 K_s-selected normal galaxies from deep infrared observations in each field. We derive the clustering lengths and linear galaxy biases of both populations, which lead to the estimation of the SMG clustering length of $r_0 \sim 4 - 5\ h^{-1}$ Mpc. We find that SMGs do not cluster strongly as reported in previous studies, occupying dark matter halo mass of $M_\mathrm{halo} \sim 10^{12}\ M_\odot$.

Key words: galaxies: evolution — galaxies: clusters — galaxies: high-redshift — submillimeter: galaxies

doi:10.6342/NTU201800137

doi:10.6342/NTU201800137

Contents

doi:10.6342/NTU201800137

doi:10.6342/NTU201800137

List of Figures

doi:10.6342/NTU201800137

doi:10.6342/NTU201800137

doi:10.6342/NTU201800137

doi:10.6342/NTU201800137

List of Tables

doi:10.6342/NTU201800137

doi:10.6342/NTU201800137

Chapter 1

Introduction

Submillimeter galaxies (SMGs) are a population of galaxies emit strongly in the far-infrared submillimeter wavebands and are ultraluminous infrared galaxies (ULIRGs; e.g., Smail et al. 1997; Barger et al. 1998; Hughes et al. 1998; Blain et al. 2002). They generally have high redshifts, with a redshift distribution appearing to peak at $z \sim 2.5$ (e.g., Chapman et al. 2003, 2005; Wardlow et al. 2011), so that SMGs are at their commonest around the same epoch as the peak in powerful active galactic nuclei (AGN) and quasi-stellar objects (QSOs). There are lots of recent works trying to investigate the evolutionary relationship across SMGs and other type of galaxies (e.g., Richards et al. 2006; Assef et al. 2011;Hickox et al. 2012). The immense far-infrared luminosities of SMGs are believed to arise from intense, but highly obscured, gas-rich starbursts (e.g., Alexander et al. 2005; Greve et al. 2005; Tacconi et al. 2006, 2008; Pope et al. 2008; Ivison et al. 2011), suggesting that they may represent the formation phase of the most massive local giant ellipticals (e.g., Eales et al. 1999; Swinbank et al. 2006).

To find the local counterpart of SMGs is indeed a very interesting problem, but it become complicated when ones try to compare across different populations. The behavior of each type of galaxies across different wavebands is unpredictable, we cannot find a single parameter that governs for all populations. For example, the stellar masses of both QSOs and SMGs are difficult to measure reliably due to either the brightness of the nuclear emission in the QSOs (e.g., Croom et al. 2004; Kotilainen et al. 2009) or strong dust obscuration of the SMGs (e.g., Hainline et al. 2011; Wardlow et al. 2011). SMGs have

doi:10.6342/NTU201800137

also found to potentially consists of complex star formation histories, while at the same time the details of the high redshift star formation that produce local massive elliptical galaxies are still poorly constrained (e.g., Allanson et al. 2009).

Another possibility is to compare source populations via the masses of their central black holes. For QSOs and the population of SMGs that contain broad-line AGN, the black hole mass can be estimated using virial techniques based on the broad emission lines (e.g., Vestergaard 2002; Peterson et al. 2004; Kollmeier et al. 2006; Vestergaard and Peterson 2006; Shen et al. 2008). Such studies generally find that SMGs have small black holes relative to the local black hole–galaxy mass relations (e.g., Alexander et al. 2008; Carrera et al. 2011), while the black holes in $z \sim 2$ QSOs tend to lie above the local relation, with masses similar to those in local massive ellipticals (e.g., Bennert et al. 2010; Decarli et al. 2010; Merloni et al. 2010). These results suggest that SMGs represent an earlier evolutionary stage, prior to the QSO phase in which the black hole reaches its final mass (e.g., Hickox et al. 2011). However, high redshift virial black hole mass estimates are highly uncertain (e.g., Marconi et al. 2008; Fine et al. 2010; Netzer and Marziani 2010) and may suffer from significant selection effects (e.g., Lauer et al. 2007; Kelly et al. 2010; Shen and Kelly 2010), and so conclusions about connections between populations are necessarily limited.

One of the recent approaches to avoid the difficulties above is through understanding the clustering scheme. Spatial correlation measurements provide information about the characteristic bias and hence mass of the halos in which galaxies reside (e.g., Kaiser 1984; Bardeen et al. 1986), and so provide a robust mass estimate that is free from observations limitations that attempting to measure stellar or black hole masses. The observed clustering of SMGs can thus allow us to directly place this population in the evolutionary history of galaxies, to test whether they reside in similar halos and may co-evolve into each other in very short time scales, as reported the starburst and ultraluminous nature of SMGs as well as the QSOs and AGNs. With knowledge of how halos evolve over cosmic time (e.g., Lacey and Cole 1993; Fakhouri et al. 2010), we can also explore the links to modern elliptical galaxies (e.g., Overzier et al. 2003), as well as the higher redshift progenitors of

doi:10.6342/NTU201800137

SMGs.

Clustering measurements can provide constraints on theoretical studies that explore the nature of SMGs in a cosmological context. Recent models for SMGs as relatively long-lived (> 0.5 Gyr) star formation episodes in the most massive galaxies, driven by the early collapse of the dark matter (here after DM) halo (Xia et al. 2012), or powered by steady accretion of intergalactic gas (Davé et al. 2010), yield strong clustering for bright sources (850 μm fluxes > a few mJy) with spatial correlation lengths $r_0 \sim 10\ h^{-1}$ Mpc. In contrast, models in which SMGs are short-lived bursts in less massive galaxies, with large luminosities produced by a top-heavy initial mass function, predict significantly weaker clustering with $r_0 \sim 6\ h^{-1}$ Mpc (Almeida et al. 2011).

There have been lots of studies on measuring the clustering of SMGs. One of the attempt is to measure the two-dimensional correlation function over the fields of interest, either by angular correlation or projected angular correlation (Scott et al. 2002; Borys et al. 2003; Webb et al. 2003; Weiß et al. 2009; Lindner et al. 2011; Williams et al. 2011; Hickox et al. 2012). A recent work is from Williams et al. (2011) who analyzed an 1100 μm survey of a region of the COSMOS field and placed 1σ upper limits on the clustering of bright SMGs (with apparent 870 μm fluxes $\geq$ 8–10 mJy) of $r_0 =$ 6–12 h^{-1} Mpc. For similarity Weiß et al. (2009) and Hickox et al. (2012) have used contiguous extragalactic 870 μm survey of the Extended Chandra Deep Field-South (ECDFS) to derive the clustering of bright SMGs from their projected distribution on the sky. The former estimated a correlation length of $r_0 = 13 \pm 6\ h^{-1}$ Mpc with SMGs ≥ 5mJy. The latter has reached a more robust conclusion that SMGs exhibit strong clustering with $r_0 = 7.7^{+1.7}_{-2.3}\ h^{-1}$ Mpc. Other work has attempted to improve on angular correlation measurements by including accurate redshift information. Blain et al. (2004) estimated an effective correlation length of $r_0 = 6.9 \pm 2.1\ h^{-1}$ Mpc, using the spectroscopic redshift survey of 73 SMGs with 870 μm fluxes of $\geq$ 5mJy spread across seven fields from Chapman et al. (2005) work. Blake et al. (2006) has computed the angular cross-correlation between SMGs and optically selected galaxies by using data from the Great Observatories Origins Deep Survey-North (GOODS-N, Giavalisco et al. 2004). They made assumption that both samples tracing

doi:10.6342/NTU201800137

the same population of halos and grouped them in identical photometric redshift slices. They suggested that SMGs are more strongly clustered than the optically selected galaxies (stronger bias), although with only marginal $\sim 2\sigma$ significance.

Previous works have pointed toward SMGs being a strongly clustered population. However, recent works show different results. Wilkinson et al. (2017) used the largest SMGs population up to date in the UKIDSS UDS field ($N_{\rm SMG} \sim 300$) and obtain a relatively smaller correlation length and bias ($r_0 = 4.1^{+2.1}_{-2/0}\ h^{-1}$ Mpc and $b = 2.1 \pm 0.97$). They find that low redshift SMGs and those with faint radio counterparts may dilute the clustering result. Another factor worth noting is that clustering measurements performed with single-dish surveys are subject to the so-called “blending bias” (hereafter $b_{\rm b}$), as reported in Cowley et al. (2017). This describes the contribution to the clustering signal due to the blending of multiple SMGs into single submillimeter sources as a result of the low angular resolution of single-dish telescopes. This effect boosts the measured galaxy bias and therefore magnifies the derived halo mass, which has to be corrected in future works.

To improve measurements of the clustering of SMGs up to this end, we need either much larger survey areas and number of sources or the inclusion of accurate redshift information. We use the latest 850 μm observations by Submillimeter Common-User Bolometer Array 2 (SCUBA-2) camera located on the 15 m James Clerk Maxwell Telescope (JCMT) on GOODS fields. The SCUBA-2 data were obtained by Cowie et al. (2017) through the program “SUbmillimeter PERspective on the GOODS fields (SUPER GOODS)”. Although the fields area coverage is smaller and number of detected SMGs is less than in Hickox et al. (2012) and Wilkinson et al. (2017), this survey detected very faint SMGs, pushed the 850 μm flux density detection to the deepest end. Therefore it is possible to investigate the clustering properties of faint SMGs by using the SUPER GOODS data. Limited number of SMGs induces large shot noise in angular autocorrelation analysis, we apply the angular cross-correlation analysis on SMGs and less-active normal galaxies to estimate the spatial clustering length and galaxy bias. We expect this result to give a rough estimate on the SMG clustering feature, as well as the halo mass SMG resides.

doi:10.6342/NTU201800137

The content of this thesis is organized as follows. In Section 2 we introduce the SMG and galaxy samples, and in Section 3 we give an overview of the methodology used to calculate correlation functions. In Section 4 we present the results and discuss our results. In Section 5 we summarize our conclusions. Throughout this paper we assume a flat cosmology with $\Omega_{\rm m} = 0.3$, $\Omega_{\Lambda} = 0.7$, $\Omega_{\rm b} = 0.05$. For direct comparison with other works, we assume $H_0 = 100\ h$ kms^{-1}Mpc^{-1} where $h = 0.7$. For the need of power spectrum we use values of $\sigma_8 = 0.84$ and spectral index $n_{\rm s} = 0.95$. All quoted uncertainties are 1σ (68% confidence).

doi:10.6342/NTU201800137

doi:10.6342/NTU201800137

Chapter 2

SMG and Galaxy Samples

There have been several studies on SMG clustering in recent years in different fields, such as UKIDSS, COSMOS, ECDFS etc. In this work we focus on the GOODS fields. In these fields there exist very deep submillimeter observations and large SMG sample sizes, making possible to conduct clustering studies in relatively small regions. To conduct the cross-correlation analysis, we need a background galaxy population. We therefore use the deep infrared observations in these two fields, particularly the K_s-band normal galaxy (inactive, excluding AGNs) catalogs.

2.1 SMG Sample

Our SMG sample comes from the deep SCUBA-2 survey of the GOODS fields (SUbmillimeter PERspective on the GOODS fields: SUPER GOODS) at 850 μm wavelength space (Cowie et al. 2017). The survey centered on the GOODS-N and GOODS-S fields, with a total mapping area of about 450 arcmin^2, reaching a central *rms* noise of 0.28 mJy. In order to reach the maximum depth at the central region as well as to cover brighter but rarer sources in the outer regions, the observations have been conducted with different scanning methods, resulting in images with increasing noise toward the edge. This gives a total of 208 and 146 SMGs at $> 4\sigma$ significance in the GOODS-N and GOODS-S, respectively (see Fig. 2.1 on page 9).

doi:10.6342/NTU201800137

Due to the non-uniformed distribution of noise level, we apply a threshold to avoid apparent clustering figure naturally arising from the lower noise near the center of the images. The confusion limit of SCUBA-2 detection in the SUPER GOODS has reached down to ~ 1.6 mJy (see Fig. 2.2 on page 10). To maintain a reliable detection, we therefore apply both a noise and a flux cut, which are 0.5 mJy and 2.0 mJy (4 σ detection) respectively, to create a uniformed selection of sources across the fields. The noise and flux thresholds are chosen to reach the deepest and faintest end of this survey, but also to retain the maximum number of SMG for the sake of correlation analysis. In conclusion, we require a noise level region with $\sigma_{\mathrm{rms}} < 0.5$ mJy and $S_{850} > 2.0$ mJy (see Fig. 2.4 on page 11), and we are then left with 76 and 67 SMGs in GOODS-N and GOODS-S respectively, which are by far the largest number of SMGs with this depth. Our samples consist of many faint SMGs with $S_{850} < 4$ mJy (see Fig. 2.3 on page 10). Note that although Cowie et al. (2017) included photometric redshifts for some SMGs, we do not use them because of the great uncertainty in the redshift measurement. We will explain the usage of redshift in the next section.

2.2 Redshift Distribution of SMGs

The redshift distribution and evolution of SMGs have been extensively studied in recent years to uncover their natures. However, SMGs are often faint in optical or near-infrared passbands, and have poorly constrained positions in the low-resolution single-dish maps ($18''$ for SCUBA-2), making it extremely challenging to identify their optical counterparts as well as redshifts. Cowie et al. (2017) published the SMGs catalogs which provide spectrometric redshifts when available, and they found that most SMGs in GOODS lie in $z \sim 2 - 5$. However, we do not include them in our study because the number of redshifts are too limited for further analysis. Recently Simpson et al. (2014) derived the photometric redshift distribution for 870 μm SMGs in the ECDFS with robust identifications based on the observations with ALMA; they modeled SEDs of all detected SMGs and gave a log-normal redshift distribution with median $\bar{z}_{\mathrm{phot}} = 2.5 \pm 0.2$, which is similar

doi:10.6342/NTU201800137

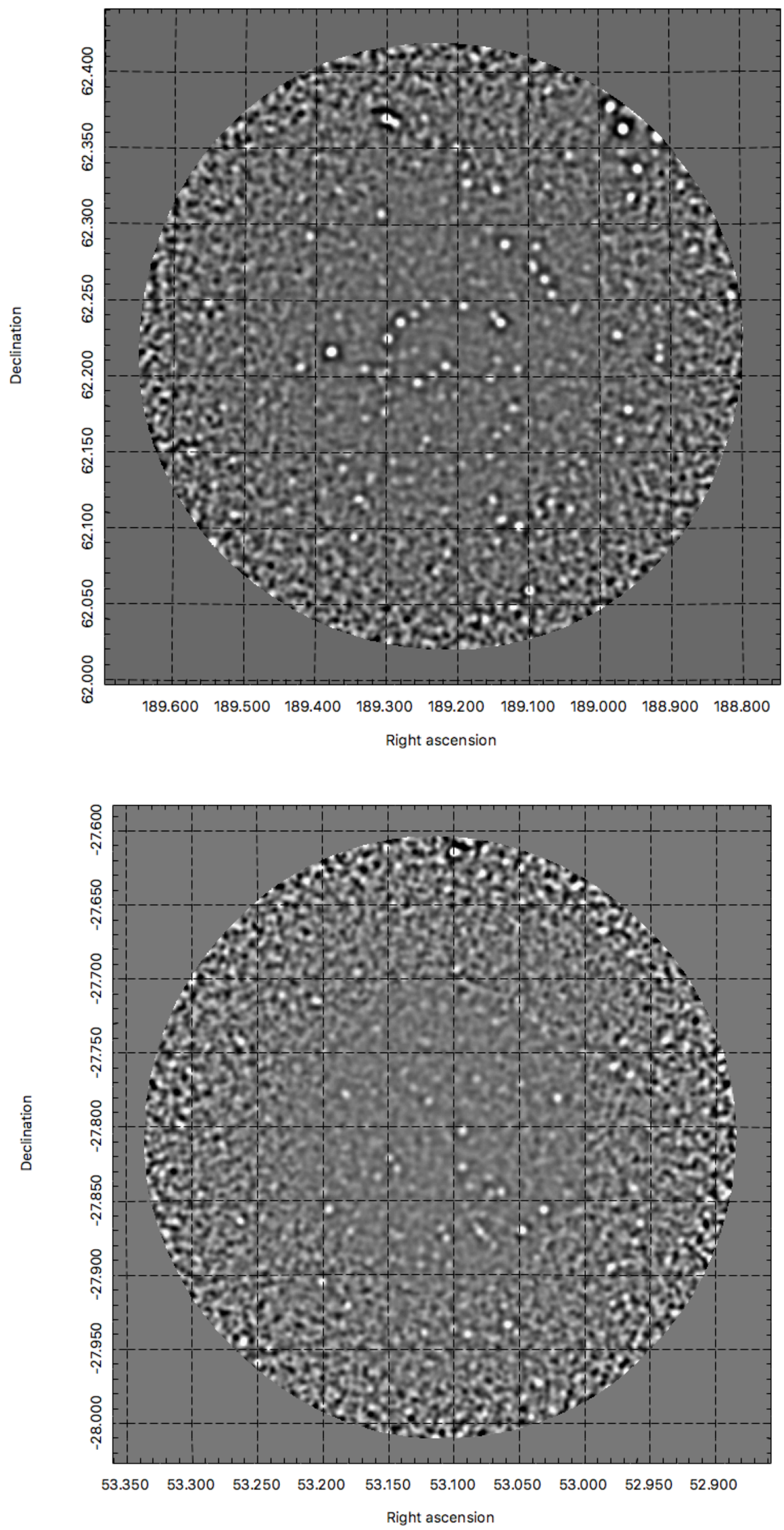

Figure 2.1: (a) GOODS-N 850 μm matched-filter S/N image. (b) GOODS-S 850 μm matched-filter S/N image.
Both maps have radii about $10'$.

doi:10.6342/NTU201800137

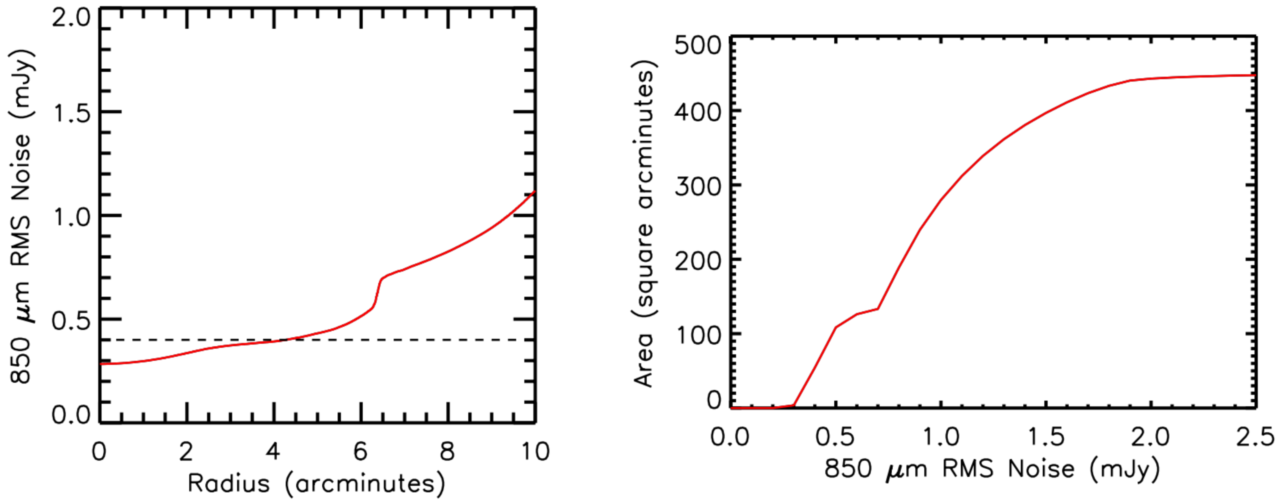

Figure 2.2: GOODS-N noise distribution, adopted from Cowie et al.(2017, their Fig. 1).
(a) Azimuthally averaged 850 space after 850 μm rms noise vs. radius. The more sensitive central region (radius less than 6′) is dominated by the CV Daisy observations, while the outer region is covered by the PONG-900 observations. The black dashed line shows the rms noise corresponding to a 4 σ detection threshold of 1.6 mJy, the approximate confusion limit for the JCMT at 850 μm.
(b) Cumulative area covered vs. 850 μm rms noise.

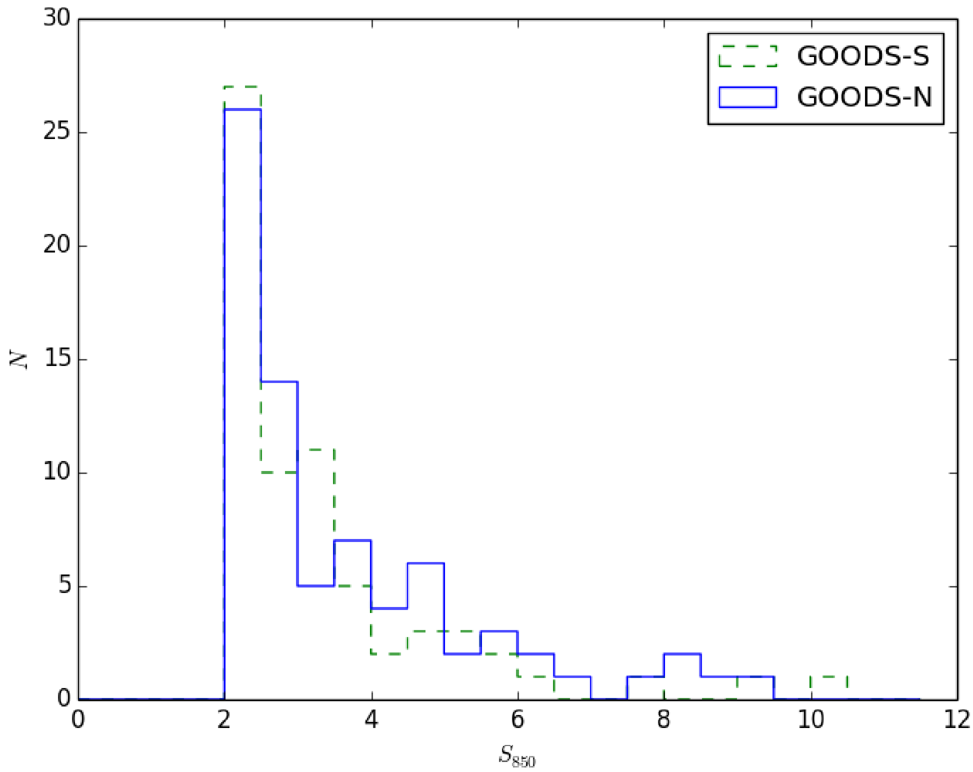

Figure 2.3: SMG 850 μm flux density distribution. Blue solid line is the GOODS-N SMGs flux distribution while green dotted line is for GOODS-S. The cut on 2 mJy is to avoid artificial clumping of sources due to observation pattern. Obviously our sample includes many faint SMGs $S_{850} < 4$ mJy.

doi:10.6342/NTU201800137

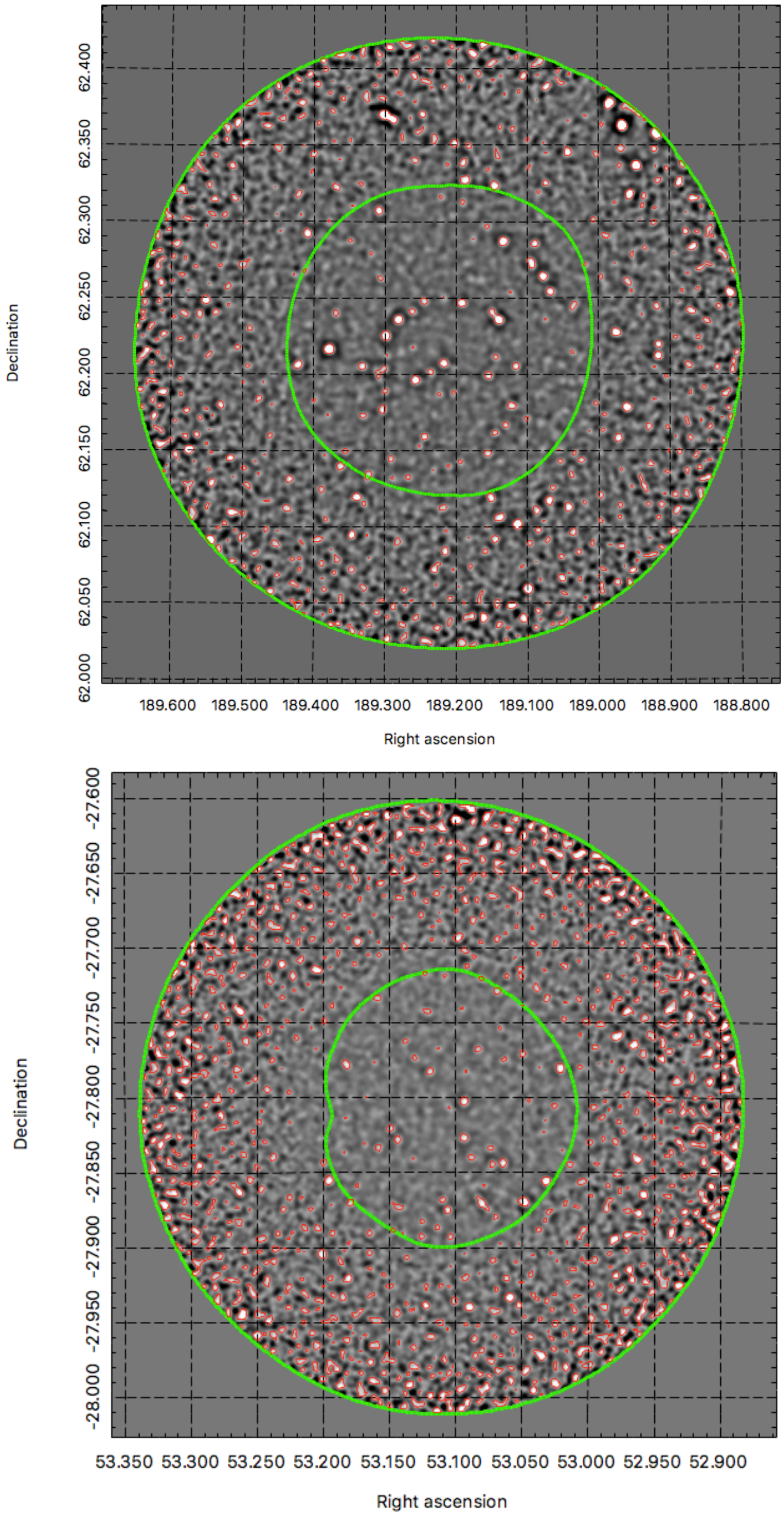

Figure 2.4: (a) GOODS-N SMG sources map. (b) GOODS-S SMG sources map. The inner green contour level is where $\sigma_{\rm rms} = 0.5$ mJy. The red contour is the flux cut of $S_{850} = 2.0$ mJy. Note that the surface density of sources is higher in the central low S/N region of the image. To account the apparent clumping toward the image center due to the observation method, we apply noise and S_{850} threshold cut on the image, remove the centermost faintest sources so that those relatively fainter S_{850} sources are also detectable at outer region.

doi:10.6342/NTU201800137

to that in previous studies (Chapman et al. 2005; Wardlow et al. 2011),

$$\left.\frac{dN}{dz}\right|_{\mathrm{ALESS}} \propto \frac{1}{(z-1)\sigma_{\mathrm{z}}} e^{-\left[(\ln(z-1)-\mu)^2/(2\sigma_z^2)\right]}.$$

See Fig. 2.5 on page 13. The latest study from Brisbin et al. (2017) confirmed this result for SMGs redshift distribution in the COSMOS field. Here, we simply assume our target sample SMGs to follow the same redshift distribution, i.e., a log-normal distribution with $\mu = 1.5$, $\sigma_z = 0.59$ and $\bar{z} = 2.5$, restricted within the range of $z = 1 - 3$ where most SMGs are found to locate,

$$\left.\frac{dN}{dz}\right|_{\mathrm{GOODS}} \propto \frac{1}{(z-1)\sigma_{\mathrm{z}}} e^{-\left[(\ln(z-1)-(\mu-1))^2/(2\sigma_z^2)\right]}.$$

2.3 K_{s} Galaxy Sample

Our GOODS-N normal galaxies are selected from the ultradeep K_{s}-band catalogs published by Wang et al. (2010). Covering 0.5×0.5 degree^2 area with the depth up to $K_{\mathrm{S,AB}} = 26.79$, it provides the most complete catalog for our analysis in this region. This survey does not include redshift information of the normal galaxies in the field, so we obtain the photometric redshifts of normal galaxies from the catalogs included in Rafferty et al. (2011). It includes data from multiwavelength observations, covering optical to radio wavebands. These sources are cross-matched with the K_{s}-band data by using a matching radius of $1''$, which is larger than the positional uncertainty of the catalogs to achieve the maximum usage of the normal galaxies .

Our GOODS-S normal galaxies are selected from the catalog published by Hsu et al. (2014). They included the most recent data in Cosmic Assembly Near-IR Deep Legacy Survey (CANDELS) and the Taiwan ECDFS Near-Infrared Survey (TENIS; Hsieh et al. 2012). The results of his high-quality survey results provide accurate positions and photometric redshifts with detailed probability density functions (PDFs) of K_{s} galaxies. With the TENIS coverage on 0.5×0.5 degree^2 area and limiting magnitude up to $K_{\mathrm{S,AB}} = 29.93$,

doi:10.6342/NTU201800137

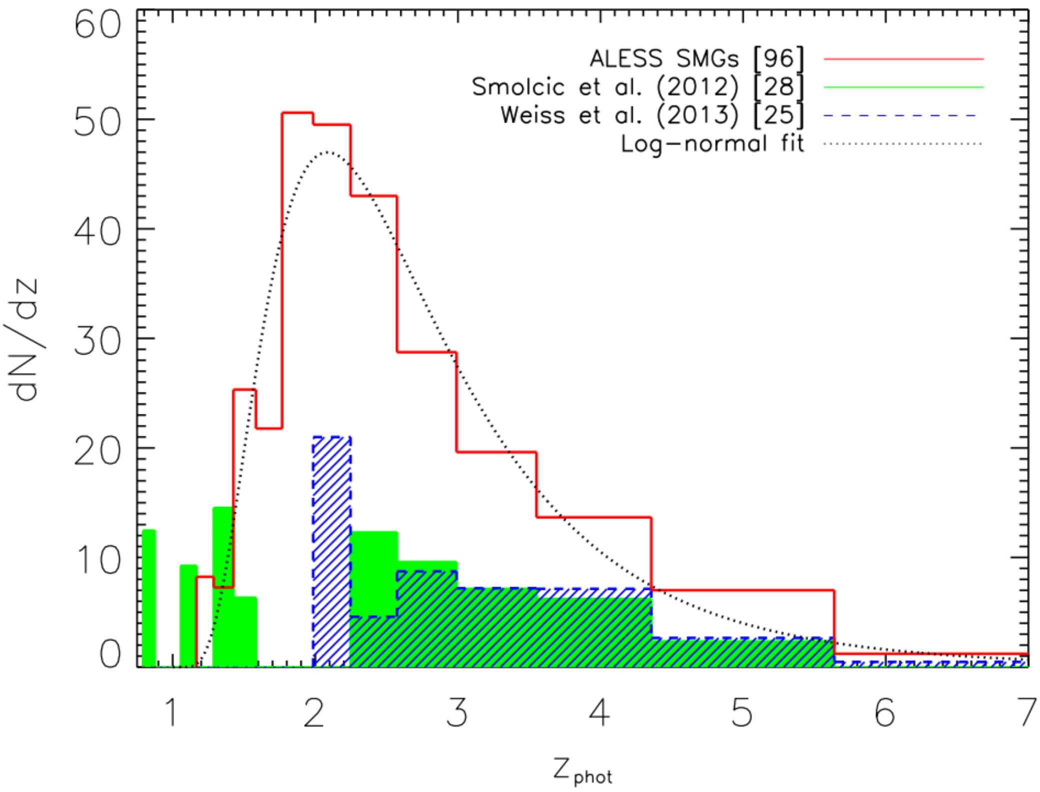

Figure 2.5: The redshift distribution of the ALESS SMGs, adopted from Simpson et al. (2014, their Fig. 12).

The redshift distribution binned uniformly in time, and normalized by the width of each bin. Simpson et al. (2014) find the redshift distribution is well-represented by a log-normal distribution with $\mu = 1.53 \pm 0.02$ and $\sigma_z = 0.59 \pm 0.01$. For comparison they show the redshift distribution from Smolčić et al. (2012), an interferometric study of 28 millimeter-selected SMGs, containing spectroscopic and photometric redshifts. They also show the spectroscopic redshift distribution from a similar interferometric study of 25 millimeter-selected lensed SMGs from Weiß et al. (2013), choosing the robust or best-guess redshifts from their analysis. They note that they have included the lensing probability as function of redshift, given in Weiß et al. (2013), in the distribution. The SMG samples presented have selection functions that are difficult to quantify (especially the lensed sample of Weiß et al. (2013)), and hence do not have a well defined survey area. In contrast to the previous studies, the redshift distribution of the ALESS SMGs does not show evidence of a flat distribution between $z \sim 2$–6, and displays a clear peak in the distribution at $z = 2$.
Brisbin et al. (2017) separately reported the similar phenomena for SMGs in COSMOS field, strengthen the reliability to use this redshift distribution in this study.

doi:10.6342/NTU201800137

it also provides the most detailed catalog for our analysis.

2.4 Redshift Selection and Mask Effect

For this study, we restrict our analysis to the K_s galaxies with redshifts of $z = 1 - 3$. The upper limit of $z = 3$ is included to maximize the overlap in redshift space with the SMG sample so that we could obtain significant correlation signal, while the lower bound of $z = 1$ is to prevent the correlation signal from being biased toward low redshifts where SMGs are rare.

It should be noted that we do not include the probability distribution function (PDF) of redshift in the whole work, since the use of redshift PDF complicates the work. We use spectroscopic redshift only when provided, otherwise the single best-derived photometric redshifts from the catalogs are used for the K_s galaxies instead.

To perform cross-correlation analysis in the field, we need to apply the same selection mask for all populations regarded. For the correlation analysis, we require random catalogs of galaxies at random positions across the fields. GOODS fields contain several bright stars with large holes, where very few galaxies are detected in the catalogs. We create a mask according to it, and apply the mask to random catalogs, SMGs, and the K_s galaxies so that the positions of the random galaxies would be unbiased with respect to the SMG and K_s galaxy samples, thus the correlation analysis would be unaffected by the holes. The final images are as shown in Fig. 2.6 on page 15, with an area ~ 100 arcmin^2 (radius $\sim\ 6'$). The resulting GOODS-N photometric catalog comprises a total of 2978 sources while 12% have z_spec , and GOODS-S comprises 2407 sources while 20% have z_spec. Furthermore, SMGs sample have reduced to 75 and 66 in GOODS-N and GOODS-S, respectively. We summarize the number of galaxies used in Table 2.1.

Field	GOODS-N		GOODS-S	
Galaxy	SMG	K_s galaxies	SMG	K_s galaxies
Original size	208	15750	146	18713
Final size	75	2978	66	2407

Table 2.1: Galaxy samples used in this study. We choose SMGs with $S_{850} > 2$mJy and $\sigma < 0.5$mJy. Infrared K_s normal galaxies (5σ) are chosen to reside in the same area coverage, with $1 < z < 3$.

doi:10.6342/NTU201800137

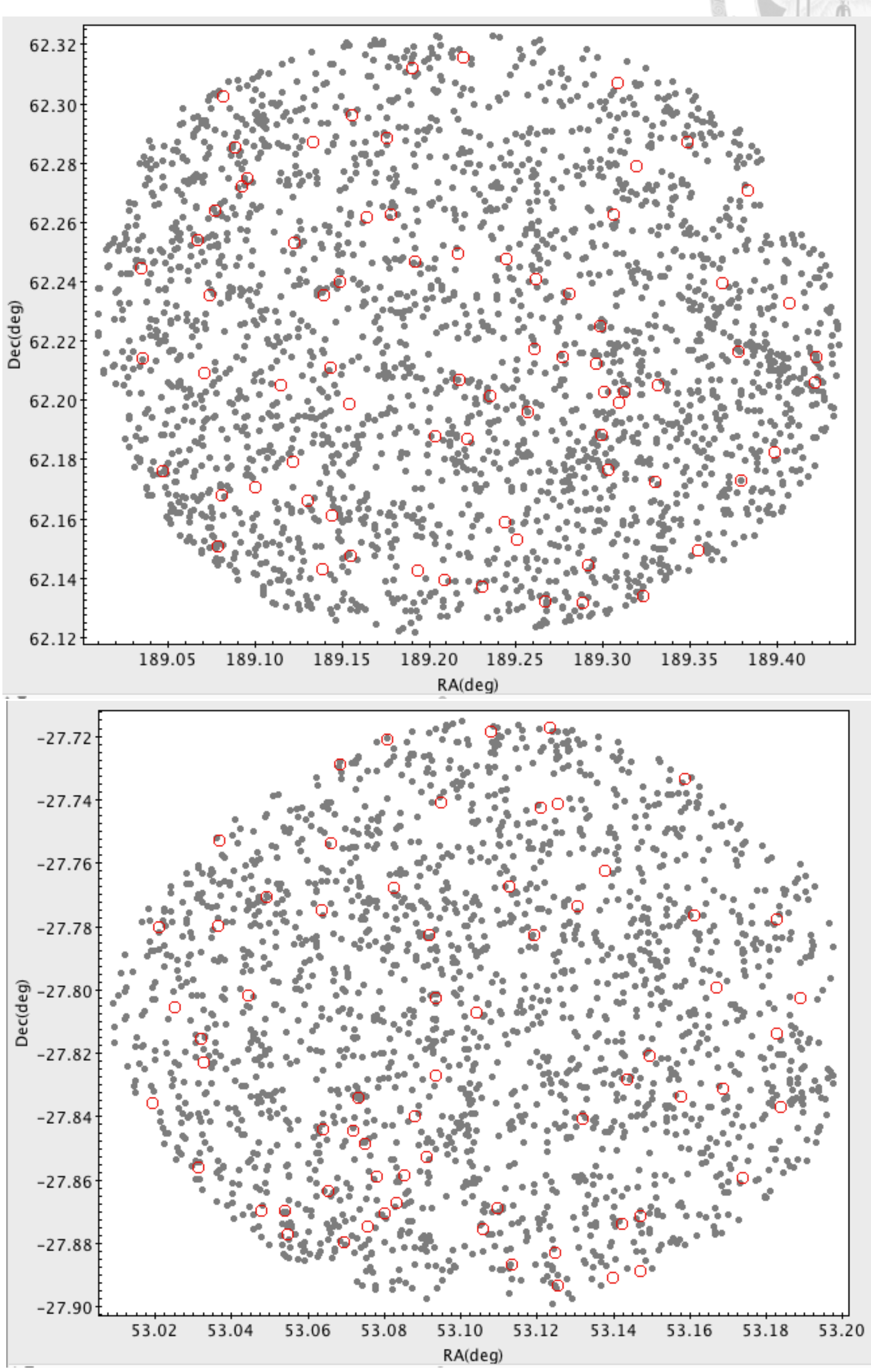

Figure 2.6: (a) GOODS-N (b) GOODS-S
Two-dimensional distribution of SMGs and infrared normal K_s galaxies in GOODS fields that are used in our analysis. The SMGs shown represent the subset of the full samples SMGs that have matched the noise and threshold cut. The K_s galaxies are chosen to reside at $z = 1-3$ with $5\,\sigma$ detection. The SMGs are shown here individually with red circles while galaxies are in gray points. The blank areas represent the regions which are excluded from the analysis, i.e., around bright stars where few galaxies have been detected.

doi:10.6342/NTU201800137

doi:10.6342/NTU201800137

(watermark seal of National Taiwan University)

Chapter 3

Correlation Analysis

In this section, we outline our methods for measuring the angular cross-correlation between SMGs and galaxies, the autocorrelation of the galaxies, the absolute bias and characteristic DM halo mass.

3.1 Correlation Method

To analyze the clustering properties of galaxy populations, we evaluate the two-point correlation function. The two-point correlation function can be measured by counting the number of unique galaxy pairs as a function of separation and comparing the resulting distribution to that of a catalog of random points with the same number density and subject to the same observing geometry. Because we detect galaxies on a two-dimensional surface, we use the angular correlation function, a projection of the three-dimensional spatial correlation function (Peebles 1980). The two-point correlation function provides us a robust way of tracing the dependence of large-scale structure on galaxy properties and evolution through redshift. Several estimators for the angular two-point correlation functions are available, we use the Landy and Szalay (1993) estimator for observed angular correlation function (hereafter ω_{obs}), which have shown to have minimum variance and bias, as described by

$$\omega_{\text{obs}}(\theta) = \frac{DD(\theta) - 2DR(\theta) + RR(\theta)}{RR(\theta)}, \tag{3.1}$$

doi:10.6342/NTU201800137

where $DD(\theta)$, $DR(\theta)$ and $RR(\theta)$ are the galaxy-galaxy, galaxy-random and random-random normalized pair counts, respectively.

However, since the angular correlation is the *excess* probability of finding a data pair versus finding a random pair, as the data pairs decrease over distance the normalized number of random pairs is greater than the number of data pairs, ω_{obs} cannot be positive for all θ. Therefore, in field of finite size, estimators of the correlation function based on pair counts are subject to the integral constraint, which can be expressed as (Groth and Peebles 1977)

$$\int\int \omega_{\text{obs}}(\theta_{12})\, d\Omega_1 d\Omega_2 \simeq 0, \tag{3.2}$$

where θ_{12} is the angle between the solid angle elements $d\Omega_1$ and $d\Omega_1$ and the integrals are over the survey area. The size of this bias increases with the clustering strength and decreases with field size; in our very small field studies, it is a significant effect and a correction must be made. The integral constraint correction is approximately constant and equal to the fractional variance of galaxy counts in a field,

$$\text{IC} \approx \frac{1}{\langle N_{\text{gal}} \rangle} + \omega_\Omega, \tag{3.3}$$

where the first term on the right is the Poisson variance and the second accounts for the additional variance caused by clustering (Peebles 1980),

$$\omega_\Omega = \frac{1}{\Omega^2} \int\int \omega(\theta_{12}) d\Omega_1 d\Omega_2, \tag{3.4}$$

In this study we consider the latter term ω_Ω only since it dominates the integral constraint. ω_Ω is dependent on the intrinsic clustering of galaxies, normally by adopting some form for $\omega(\theta)$. We use the formalism of Roche and Eales (1999),

$$\omega_\Omega = \frac{\sum RR(\theta)\omega(\theta)}{\sum RR(\theta)}. \tag{3.5}$$

Numerous studies have shown that most galaxy populations obey power law approx-

doi:10.6342/NTU201800137

imation on the angular correlation function (hereafter ACF),

$$\omega(\theta) = A\left(\frac{\theta}{1\,\mathrm{rad}}\right)^{-\delta}. \tag{3.6}$$

Adopting power law form of ACF, the resulting correlation returns

$$\omega_{\mathrm{obs}} = A\left(\theta^{-\delta} - \frac{\sum RR(\theta)\theta^{-\delta}}{\sum RR(\theta)}\right). \tag{3.7}$$

The second term in the bracket is the geometric feature of field studied, which we name C hereafter if mentioned. The uncertainty in the Landy and Szalay estimator can be estimated by assuming that $DD(\theta)$ has Poisson variance, in this case

$$\sigma_{\mathrm{obs}}(\theta) = \frac{1+\omega(\theta)}{\sqrt{DD(\theta)}}. \tag{3.8}$$

Derive the ACF on small sample (number of SMG $\sim 10^2$) is expected to produce very large statistical errors, reducing our ability to derive well-constrained clustering properties (Chen et al. 2016). However, we can apply a closely related correlation function: the two-point cross-correlation function (CCF), by using the larger sample of K_{s}-band selected galaxies in the same field. We cross-correlate the target sample galaxies (D_{s}) with the tracer galaxies (D_{t}), as follows:

$$\omega_{\mathrm{obs}}(\theta) = \frac{D_{\mathrm{s}}D_{\mathrm{t}}(\theta) - D_{\mathrm{s}}R(\theta) - D_{\mathrm{t}}R(\theta) + RR(\theta)}{RR(\theta)}, \tag{3.9}$$

where both data sets are normalized by the total pair counts. By cross-correlating a small target sample (SMGs) with a large tracer population (K_{s} tracer galaxies, we explain the subset selection in next section), we significantly increase the number of pairs, reaching greatly reduced statistical uncertainties, compared to directly derive the ACF of SMGs alone.

doi:10.6342/NTU201800137

3.2 Tracer Galaxy Subset

To understand the clustering feature of SMGs we first apply the ACF on K_s galaxies. The larger sample size enables us to derive the clustering properties from ACF alone. The galaxy autocorrelation varies with redshift, owing to the evolution of large-scale structure. In our study we choose K_s galaxies with magnitude $24.5 > m_{K_s} > 19.5$ with 5σ detection. This is done to remove galaxies with marginal flux detection that may arise due to false detection. This selection has been done in both GOODS fields. The use of flux-limited sample however means that we select more luminous galaxies in high redshift regions. These fewer luminous high-z infrared galaxies will affect the correlation function between SMGs and K_s galaxies since they dominate the CCF where SMGs are peaked at redshift space, but have tiny effect on ACF due to their small number, shallow the strength of CCF to interpret the SMGs clustering feature. To overcome the inconsistency and improve the reliability of the CCF calculation, we random choose K_s galaxies with redshift overlap with SMGs redshift distribution in each redshift bins to enter the correlation calculation, i.e., the tracer galaxies. We have made the assumption that SMGs and tracer galaxies follow the same galaxy evolution scheme. We use this smaller tracer galaxy sample to calculate the ACF and CCF. In our analysis we model about 2000 tracer galaxies in correlation calculation to maximize usage of high-z galaxies with replacement (see Fig. 3.1 on page 21).

3.3 Uncertainties of ACF and CCF

The subset usage for K_s galaxies however means that we lose information on other galaxies excluded. The ACF result alters when we choose different tracers to enter the calculation. We employ an iteration method to minimize this effect. Firstly, we choose a tracer subset and do bootstrap resampling to give correlation function and error. Secondly, the process is iterated until the spread in correlation function in single angle bin converges and dominants over the Poisson errors, therefore we combine all measurements to obtain the mean and the uncertainty. The same strategy has been applied on CCF calculation.

doi:10.6342/NTU201800137

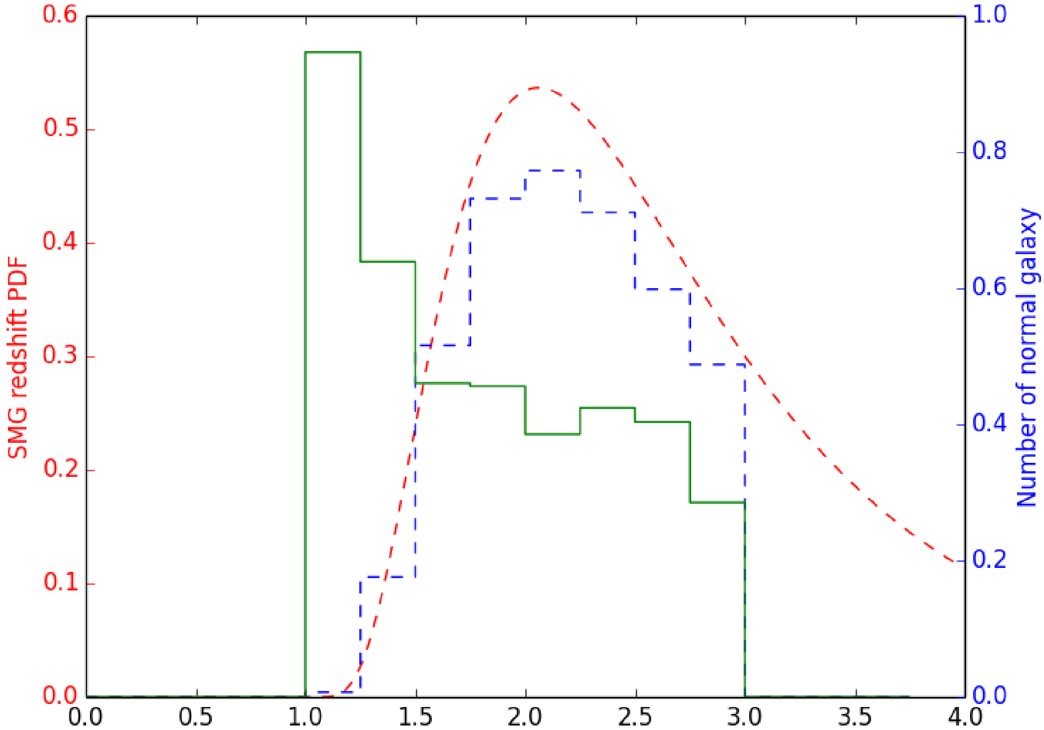

Figure 3.1: Redshift distributions for the K_s galaxy sample in the redshift range $z = 1-3$ (solid green line), and the SMG redshift distribution in the range $z = 1-4$ (dotted red line). The histograms for all populations have been scaled so that the distribution can be directly compared to each others. Also shown is the redshift distribution for tracer galaxies (dashed blue line) selected to match the overlap in the redshift distributions of the SMGs, as used in both ACF and CCF analysis. 12% in GOODS-N and 20% in GOODS-S galaxies have spectroscopic redshifts. We use $z_{\rm spec}$ if any, otherwise $z_{\rm photo}$ is used instead.

doi:10.6342/NTU201800137

The random catalogs used are always 10 times larger than the tracers throughout the whole work.

3.4 Galaxy Bias

According to the current cosmological paradigm of structure formation, galaxies form and evolve inside dark matter halos (White and Rees 1978). In other words, there exists a connection between the DM distribution and galaxies in the dense DM regions. The galaxy spatial distribution, however, is linearly biased with respect to the DM density field. The strength of this effect is referred to as *galaxy bias*, or *bias* in common. In practice, there are two ways to obtain the bias: power law method and HOD modeling. We use power law method in this study and leave HOD modeling for further discussion. One of the simplest way to obtain bias is from the *large-scale* angular correlation analysis. The linear scaling gives the *relative bias* between two galaxy types,

$$b_{12}^2 = \frac{\omega_{\text{gal1,gal2}}}{\omega_{\text{DM}}}, \tag{3.10}$$

where 1,2 represent types of galaxy, numerator the correlation function between two populations and denominator the dark matter correlation function if we assume two populations trace the same DM distribution (or DM halo mass function). Note that it reduces to absolute bias if we use the autocorrelation function in the numerator.

The mass of the DM halos in which K_{s} galaxies and SMGs reside are reflected in their absolute clustering biases relative to the DM distribution, b_{t} and b_{s} relatively. To estimate DM halo mass of SMGs, we calculate the relative bias between SMGs and K_{s} galaxies, b_{st} from which we derive the absolute bias of SMGs relative to DM, b_{s}. To determine absolute bias (following Ichikawa et al. 2007, Myers et al. 2007, Hickox et al. 2011), we first calculate the two-point autocorrelation of DM as a function of redshift. We use the HALOFIT code of Smith et al. (2003) to determine the nonlinear-dimensionless power spectrum $\Delta^2_{\text{NL}}(k, z)$ of the DM assuming our standard cosmology, and the slope of the initial fluctuation power spectrum, $\Gamma = \Omega_m h = 0.21$. We then project the power spectrum

doi:10.6342/NTU201800137

$\Delta^2_{\rm NL}(k,z)$ into the angular correlation, as shown Equation (A6) in Myers et al. (2006). The key parameter is the redshift distribution of the galaxies (SMGs and $K_{\rm s}$ galaxies), which we have assumed to be the same in our analysis (see Section 3.2 and Fig. 3.1 on page 21),

$$\frac{dN_{\rm SMG}}{dz} = \frac{dN_{\rm K_s}}{dz}. \tag{3.11}$$

For each correlation analysis we fit the correlation value to the DM $\omega_{\rm DM}(\theta)$ by minimizing χ^2 with linear scaling, as shown in Equation (3.5). This linear scaling ratio yields $b_{\rm t}^2$ for $K_{\rm s}$ galaxy ACF or $b_{\rm st}^2$ for SMG-$K_{\rm s}$ galaxy CCF. Finally, we use $b_{\rm t}$ and $b_{\rm st}$ to infer the absolute bias of SMGs in the fields through

$$b_{\rm s} = \frac{b_{\rm st}^2}{b_{\rm t}}. \tag{3.12}$$

With this linear bias $b_{\rm s}$ we infer the expected ACF of SMGs by multiplying out the tracer population bias from the CCF by $b_{\rm st}^2/b_{\rm t}^2$ or $b_{\rm s}/b_{\rm t}$, allowing us to compare the ACF of all populations.

3.5 Clustering Length r_0

3.5.1 Power Law Model: Limber's Equation to Clustering Length $r_{0,\rm SS}$

When the correlation function is expressed in power law model (default if no additional subscript), the spatial correlation function can be written as (Peebles 1980; Myers et al. 2006)

$$\xi(r,z) = \left[\frac{r}{r_0}\right]^{-\gamma}, \tag{3.13}$$

where γ is the power law slope, r_0 is the spatial clustering length if we assume no evolution with redshift in the clustering of the sample. The spatial correlation function can be integrated to yield its angular projection,

$$\omega(\theta) = A\left(\frac{\theta}{1\,\rm rad}\right)^{-\delta}. \tag{3.14}$$

doi:10.6342/NTU201800137

In the small angle approximation, we can invert Limber's equation as

$$\delta = \gamma - 1 \tag{3.15}$$

$$A = H_\gamma \frac{\int_0^\infty (dN_1/dz)(dN_2/dz) E_z \chi^{1-\gamma} dz}{\left[\int_0^\infty (dN_1/dz) dz\right] \left[\int_0^\infty (dN_2/dz) dz\right]} r_0^\gamma, \tag{3.16}$$

where $H_\gamma = \Gamma(0.5)\Gamma(0.5\,[\gamma - 1])/\Gamma(0.5\gamma)$, Γ is the gamma function, χ is the angular comoving distance, $dN_{1,2}/dz$ are the redshift distributions of the samples, $E_z = H_z/c = dz/d\chi$. The Hubble parameter H_z can be found via

$$H_z^2 = H_0^2 \left[\Omega_m (1+z)^3 + \Omega_\Lambda\right]. \tag{3.17}$$

In our analysis we have chosen flat cosmology, therefore χ reduces to the radial comoving distance. Note that $\frac{dN_1}{dz} = \frac{dN_2}{dz}$ in the ACF. Owing to the small size of SMGs which can hardly provide significant constraint on both the slope δ, or γ and the clustering amplitude A, we simply assume $\gamma = 1.8$ in analysis (e.g., Quadri et al. 2007 for ACF; Hickox et al. 2012 for CCF). We fit power law with integral constraint correction to the correlation functions using the expression above (see Equation 3.3), derive the corresponding $r_{0,\,\mathrm{SG}}$, $r_{0,\,\mathrm{GG}}$ and $r_{0,\,\mathrm{SS}}$.

3.5.2 Linear Growth Perturbation Theory (L): Large-scale Galaxy Bias to SMG $r_{\mathbf{0,SS,L}}$

Differ from the previous section, we use the evolution of large-scale mass fluctuation (with subscript L) in linear regime to determine the correlation length of SMG, $r_{0,\mathrm{SS,L}}$.(e.g., Lindsay et al. 2014; Durkalec et al. 2015). σ_R is the mass fluctuation in a comoving sphere of scale radius $R\ h^{-1}$ Mpc. Following the galaxy bias definition, we have

$$\sigma_{\mathrm{R,g}}(z) = b_\mathrm{L}(M, z)\sigma_{\mathrm{R,m}}(z), \tag{3.18}$$

where b_L is the galaxy bias. The usually adopted value for σ is $R = 8\ h^{-1}$ Mpc and in this work we use $\sigma_{8,\mathrm{m}}(z = 0) = \sigma_8 = 0.84$. In the model the redshift evolution of mass

doi:10.6342/NTU201800137

fluctuation is described as

$$\sigma_{8,\mathrm{m}}(z) = \sigma_{8,\mathrm{m}}(z=0)D(z), \tag{3.19}$$

where

$$D(z) = \frac{g(z)}{g(0)(1+z)}, \tag{3.20}$$

and $g(z)$ is the normalized *growth factor*, which describes how fast the linear perturbations grow inside with the scale factor. We write

$$g(z) = \frac{5}{2}\Omega_{\mathrm{m}z}\left[\Omega_{\mathrm{m}z}^{4/7} - \Omega_{\Lambda z} + \left(1 + \frac{\Omega_{\mathrm{m}z}}{2}\right)\left(1 + \frac{\Omega_{\Lambda z}}{70}\right)\right]^{-1}, \tag{3.21}$$

(Carroll et al. 1992) and the cosmological parameters evolves in a flat cosmology as

$$\Omega_{\mathrm{m}z} = \left(\frac{H_0}{H_z}\right)^2 \Omega_{\mathrm{m}}(1+z)^3 \qquad\qquad \Omega_{\Lambda z} = \left(\frac{H_0}{H_z}\right)^2 \Omega_{\Lambda}. \tag{3.22}$$

Since $\sigma_{8,\mathrm{g}}$ is the clustering strength of halos more massive than stellar mass M at redshift z, following Peebles (1980)

$$\sigma_{8,\mathrm{g}} = \sqrt{C_\gamma \left(\frac{r_0}{8\ h^{-1}\ \mathrm{Mpc}}\right)^{\gamma}}, \tag{3.23}$$

with

$$C_\gamma = \frac{72}{2^\gamma(3-\gamma)(4-\gamma)(6-\gamma)}, \tag{3.24}$$

where γ is the power law slope. We can retrieve correlation length r_0 as follows:

$$r_0 = 8\left(\frac{b_{\mathrm{L}}\sigma_8 D(z)}{C_\gamma}\right)^{\frac{1}{\gamma}}, \tag{3.25}$$

when we use fixed value of $\gamma = 1.8$ to imply the derived absolute bias of SMG at its median redshift to obtain the $r_{0,\mathrm{SS,L}}$.

doi:10.6342/NTU201800137

3.5.3 Difference Between Power Law Model and Linear Growth Perturbation Theory (L)

Two-point correlation functions have been widely used in studying the clustering phenomena of different galaxy populations. Following Peebles (1980), numerous works have suggested that stellar populations obey the simple power law model. In this work, the presumed hypothesis is that CCF can be used to infer SMG ACF and to derive the clustering parameters.

For the power law method, we estimate observed clustering length $r_{0,\mathrm{SS}}$ by measuring the correlation amplitude and absolute bias b_{s} by fitting the observed correlation function to the DM distribution (following Hickox et al. 2011). We obtain CCF b_{st} and A_{st} from observation then derive b_{s} and A_{s} of SMG accordingly. Firstly, to better utilize this method depends largely on the data quality, i.e., sample sizes, field of view, luminosity, catalog completeness etc. In this study we have very small sample sizes (SMG $\sim 10^2$) with the survey area of $\sim 6' \times 6'$. We obtain reasonable result with acceptable error, however this result can be doubtful due to data deficiency, which may induce unavoidable Poisson noise into the calculation, as described in the Section 3.1. Secondly, the details within the redshift distribution of populations and DM are required to obtain b_{t} / b_{st} / b_{s}, strictly restricting ACF and CCF to stick to DM-like distribution, which is only true in large-scale. Finally, SMG ACF is forced to follow power law model to derive the $r_{0,\mathrm{SS}}$, and this could lead to abnormal result if the power law model is poorly constrained on the correlation function.

On the other way around, linear growth perturbation theory can predict the large-scale evolution of mass fluctuation. We can estimate the large-scale galaxy bias b_{L} where the target population resides in at particular redshift, should we hold the accurate cosmological parameters and the observed clustering strength of the population. We can invert the relation to obtain $r_{0,\mathrm{SS,L}}$ if we get the large-scale galaxy bias b_{L}. We use $b_{\mathrm{L}} = b_{\mathrm{s}}$, meaning that the derived absolute bias of SMG in our study *equals* to the large-scale galaxy bias predicted in the linear growth regime at the $\bar{z} = 2.5$. This however is an approximated scenario only because of our small field size. The real large-scale bias could possibly be

doi:10.6342/NTU201800137

smaller in our case, where we try to infer the observed clustering strength $r_{0,\mathrm{SS,L}}$ by partly assuring the appropriateness to use large-scale bias.

These two methods should return similar correlation results when sufficient data in large-scale are included. We hereafter estimate the corresponding clustering length and derive the DM halo mass.

3.6 Dark Matter Halo Mass

To simplified the analysis, we use a bias-halo mass relation published by Sheth et al. (2001). They derived a relation between DM halo mass and large-scale bias that agrees well with the results of cosmological simulations. We use the formalism of Sheth et al. (2001) to convert b_s to M_halo at the mean redshift ($z \sim 2.5$). This characteristic M_halo corresponds to the top-hat virial mass (Peebles 1993, and references therein), in the simplified case in which all objects in a given sample reside in halos of the same mass. This assumption is justified by the fact that SMGs have a very small number density compared to the population of similarly clustered DM halos (in our case the tracer galaxies), such that it is reasonable that SMGs may occupy halos in a relatively narrow range in mass. It is worth noting that we have assumed the biases we use to derive the DM halo mass are the large-scale bias of galaxies. We explain the discrepancy further in Section 4.6.

doi:10.6342/NTU201800137

doi:10.6342/NTU201800137

Chapter 4

Results and Discussions

In this section we discuss the results of the correlation analysis and the derived spatial clustering length r_0.

4.1 K_s Galaxy ACF

We calculate the ACF of K_s galaxies for each GOODS field. The geometric feature factor C (the last term in Equation 3.7) are similar in both fields, differs only 11 %. To conduct cross-field comparison, we use the average value of $\bar{C}$ throughout correlation calculation. This $\bar{C}$ term originated from integral constraint (IC) has a significant effect at large angle separation, and IC causes the measured correlation to decay to negative at $\theta > 100''$, which is inappropriate for analysis. The tracers, K_s-selected galaxies have a positional uncertainty within $1''$ radius. Therefore we choose the interval between $2'' \leq \theta \leq 100''$ for our interest.

The observed ACF is significant on the scales from $2''$ to $100''$ (see Fig. 4.1 on page 30), and the best-fit slopes are

$$\gamma_\mathrm{N} = 1.87 \pm 0.24$$

$$\gamma_\mathrm{S} = 1.75 \pm 0.07,$$

where N and S represent GOODS-N and GOODS-S, respectively. Within the 1σ signif-

doi:10.6342/NTU201800137

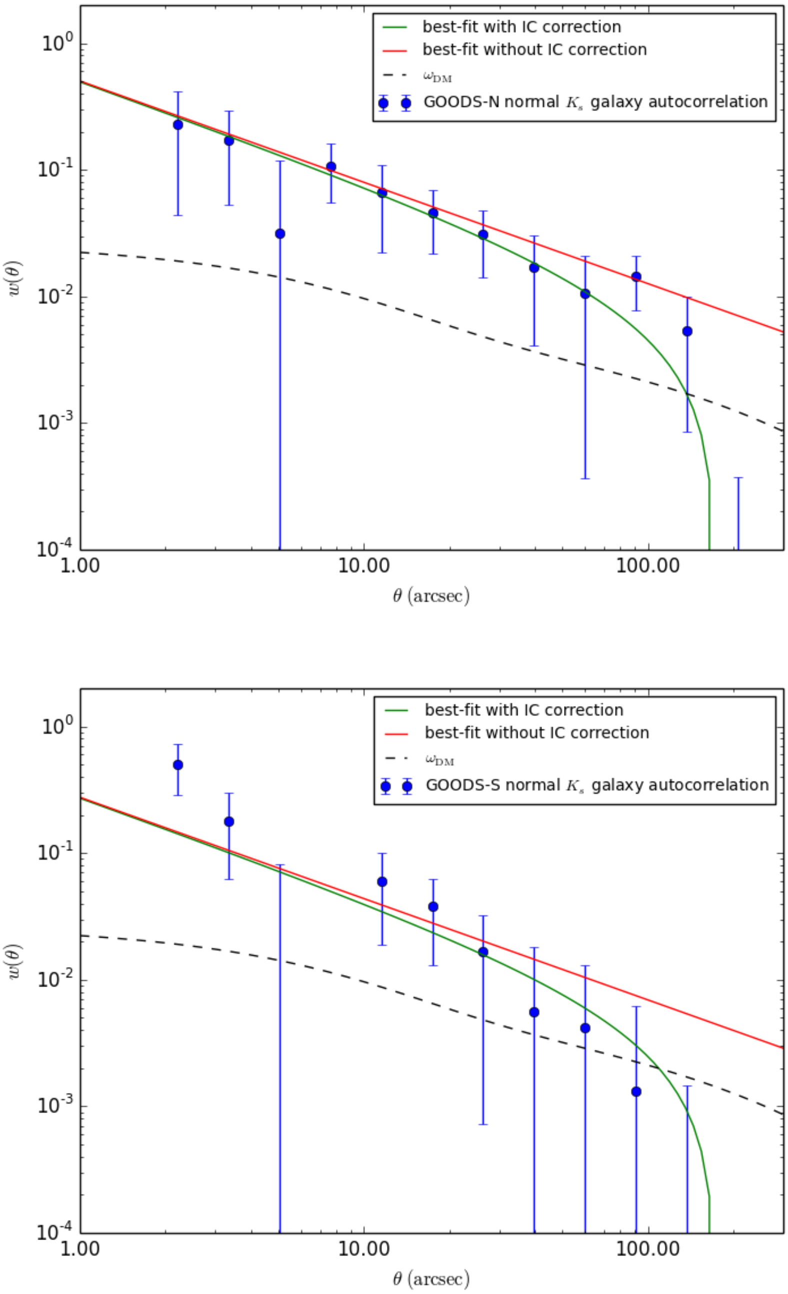

Figure 4.1: The ACF of K_s-selected normal galaxies in the GOODS fields.
Galaxies are selected to match the overlap of the SMGs and galaxies in redshift space. Uncertainties are estimated from standard deviation of the bootstrap resampling result. The ACF of DM evaluated for the redshift distribution of the galaxies is shown by the dashed black line. The power law fit is performed on scales of $2''$–$100''$ and is shown as the solid lines. The green solid line is the best-fit power law model with the integral constraint (IC, consists of geometric factor $\bar{C}$) correction while red line is the one without correction. To reduce the downsizing amplitude effect arises from small survey area, we consider angle separation smaller than $100''$. The observed amplitude of the K_s galaxy ACF yields the absolute bias b_t, which we use to obtain the absolute bias b_s and DM halo mass of the SMGs.

doi:10.6342/NTU201800137

icance they agree well with the literature value of $\gamma = 1.8$ (e.g., Peebles 1980; Roche and Eales 1999; Coil et al. 2008; Quadri et al. 2007; Ichikawa et al. (2007); Zehavi et al. 2011), so we hereafter use this fixed value unless specified. The derived spatial clustering length $r_{0,\mathrm{GG}}$ with $\gamma = 1.8$ gives

$$r_{0,\mathrm{GG,N}} = 4.45 \pm 0.32\ h^{-1}\ \mathrm{Mpc}$$

$$r_{0,\mathrm{GG,S}} = 3.18 \pm 0.68\ h^{-1}\ \mathrm{Mpc}.$$

These values are comparable with previous studies in the fields, i.e., Quadri et al. (2007), Ichikawa et al. (2007) on GOODS-N K-selected galaxy catalog (flux limited sample, high redshift) with $r_{0,\mathrm{GG,N}} \sim 4.8-6.0\ h^{-1}$ Mpc; Hickox et al. (2012) on ECDFS IRAC galaxies with $r_{0,\mathrm{GG,S}} = 3.3 \pm 0.3\ h^{-1}$ Mpc. We summarized our results in Table 4.1.

The main difference between our work and the previous studies is that we do not include redshift information in the calculation of correlation function. Redshift PDF represents the uncertainty in the redshift estimation due to the observational limitation, so by introducing the redshift PDFs as the *weighting* in the correlation method (e.g. Myers et al. 2009), one accounts all the possibilities that the target resides in redshift space. Instead of treating redshift PDFs as the statistical interpretation of observational limitation, we treat all galaxies as point targets within the redshift space. During our calculation we use the single z_{photo} or z_{spec} as the accurate redshift, intending to approach the clustering features obtained in the literature. Our result provides a first glance on the methodology application on this study, i.e., the use of accurate redshift PDF in correlation is *not* necessary to achieve acceptable and similar results.

Assume $\gamma = 1.8$,			
	GOODS	r_0 (h^{-1} Mpc)	b_{t}
K_{s} galaxies	N	4.45 ± 0.32	2.39 ± 1.34
	S	3.18 ± 0.68	1.55 ± 0.43

Table 4.1: Result of K_{s}-selected near-infrared normal galaxies ACF.

doi:10.6342/NTU201800137

4.2 SMG-K_s Galaxy CCF

Following the method introduced above, we apply cross-correlation technique on SMGs and K_s galaxies. The small number of SMGs causes large shot noise in the calculation, so we combine two GOODS fields CCF to achieve a smaller error. The result shows strong correlation on $2'' \leq \theta \leq 6''$ and $40'' \leq \theta \leq 100''$, as shown in Fig 4.2. The weak CCF signal on $\theta \sim 6'' - 10''$ was thought to originate from the mask procedure, i.e., the holes created to remove very bright sources in the fields, however the result remains unchanged after we remove the mask. Another possible reason may be the transition from 2-halo term to 1-halo term in HOD model, and we leave this in Section 4.6 for discussion.

We fix $\gamma = 1.8$ following the literature CCF studies on SMGs (Blake et al. 2006 for SMG-optically faint galaxy; Hickox et al. (2012) for SMG-IRAC galaxy). The derived clustering length returns $r_{0,\mathrm{SG}} = 5.63 \pm 0.98\ h^{-1}$ Mpc.

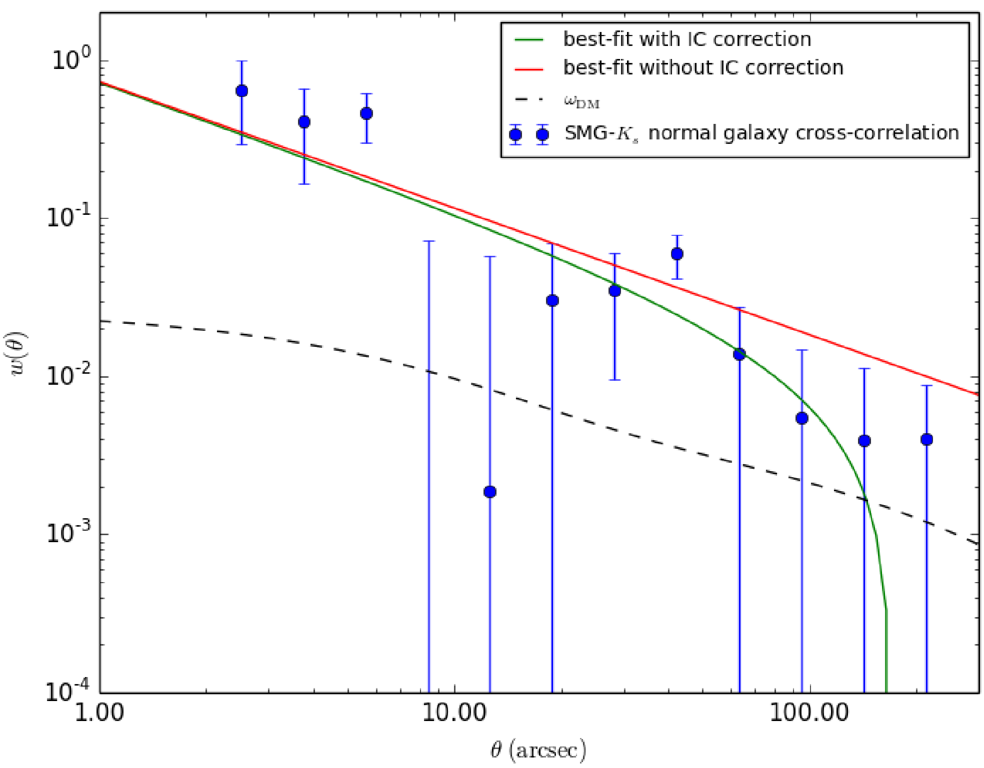

Figure 4.2: The CCF of SMG-K_s galaxy. Uncertainties are estimated from standard deviation of the bootstrap resampling result. The ACF of DM, evaluated for the redshift distribution of the SMG, is shown by the dotted black line.
The power law fit was performed on scales $2''$–$100''$ and is shown as the solid line.

doi:10.6342/NTU201800137

4.3 SMG ACF

We fit both the observed ACF and CCF with a linear scaling to $\omega_{\rm DM}(\theta)$ on the scales of $2'' - 100''$. The linear scaling of $K_{\rm s}$ galaxies (tracers) ACF corresponds to

$$b_{\rm t,N}^2 = 6.25 \pm 0.68 \qquad b_{\rm t,S}^2 = 2.39 \pm 1.34$$
$$b_{\rm t,N} = 2.50 \pm 0.14 \qquad b_{\rm t,S} = 1.55 \pm 0.43.$$

To achieve direct comparison across the GOODS fields, we combine the two tracer biases into a single tracer bias, where $b_{\rm t} = 2.02 \pm 0.23$. The fit between combined-field CCF and $\omega_{\rm DM}(\theta)$ gives $b_{\rm st}^2 = 7.34 \pm 2.81$. From this we obtain the absolute bias $b_{\rm s} = 3.63 \pm 1.45$ which is expected to be derived from an SMG ACF. We then derive the expected clustering length $r_{0,\rm SS} = 6.46 \pm 1.33\ h^{-1}$ Mpc.

The corresponding DM halo mass for each type of galaxies are given as

$$\log(M_{\rm halo,Ks}[h^{-1}\ {\rm M}_\odot]) = 11.29^{+0.25}_{-0.31}$$
$$\log(M_{\rm halo,SMG}[h^{-1}\ {\rm M}_\odot]) = 12.46^{+0.52}_{-0.98}.$$

We summarize the SMG CCF and expected ACF results in Table 4.2. The expected clustering length of SMG $r_{0,\rm SS}$ is illustrated as red star in Fig. 4.3 on page 36.

Assume $\gamma = 1.8$,					
	CCF		Expected ACF		
SMG	r_0 (h^{-1} Mpc)	$b_{\rm st}$	$b_{\rm s}$	$r_{0,\rm SS}$ (h^{-1} Mpc)	$M_{\rm halo}$ (log $h^{-1}{\rm M}_\odot$)
	5.63 ± 0.98	2.70 ± 0.51	3.63 ± 1.45	6.46 ± 1.33	$12.46^{+0.52}_{-0.98}$

Table 4.2: Result of SMG-$K_{\rm s}$ galaxy CCF and expected SMG ACF.

doi:10.6342/NTU201800137

4.4 Blending Bias Effect on The Clustering Length and DM Halo Mass

Placing bright SMGs within the broader context of galaxy formation and evolution requires accurate measurements of their clustering, which can constrain the masses of their host dark matter halos. Recent works have shown that the clustering measurements of these galaxies may be affected by a "blending bias", b_{b}. It boosts the angular correlation function of the sources extracted from single-dish imaging surveys relative to that of the underlying galaxies (Hodge et al. 2013; Karim et al. 2013; Cowley et al. 2015; Cowley et al. 2017). This is due to the confusion introduced by the coarse angular resolution of the single-dish telescopes, and could lead to inferred halo masses being significantly overestimated. In Cowley et al. (2017) work they found that the blending bias factors remain the same regardless the correlation function is derived through the ACF or CCF technique, though this can be reduced by decreasing the width of the redshift interval.

Our SMG samples originate from JCMT single-dish images, which suffer from the same blending bias. An SMG in a single-dish image may have unresolved components nearby, which increases the spatial distance to the nearest neighbor, and amplifies the correlation signal. If one obtains higher resolution images (e.g., through ALMA observations), one should expect a smaller but more accurate clustering signal, with downsizing clustering amplitude A, spatial clustering length r_0, and absolute bias b_{s}.

In our analysis we apply this blending bias correction to obtain the final result. Refer to Table 1 in Cowley et al. (2017), the ranges of our interest are $z = 1.7 - 2.8$ ($b_{\mathrm{b}} = 1.3$) and $z = 2.1 - 3.3$ ($b_{\mathrm{b}} = 1.4$). We use an average value of $b_{\mathrm{b}} = 1.35$ to remove the blending by

$$b_{\mathrm{sb}} b_{\mathrm{b}} = b_{\mathrm{s}},$$

where b_{sb} is the corrected bias after removing the blending effect.

doi:10.6342/NTU201800137

4.4.1 Power Law Method: ACF of SMG

The expected linear bias after the correction of blending bias from the SMGs ACF is $b_{\rm sb} = 2.67 \pm 1.05$. With the corrected $b_{\rm sb}$ we multiply SMGs CCF with $b_{\rm sb}/b_{\rm t}$ (see Section 3.4) to obtain the expected SMGs ACF with the respective spatial clustering length $r_{0,\rm SS,b} = 5.47 \pm 1.12\ h^{-1}$ Mpc. The clustering length of SMGs with blending correction $r_{0,\rm SS,b}$ has been shown as the blue diamond in Fig. 4.3 on page 36.

The corrected DM halo mass of SMGs is $\log(M_{\rm halo,SMG}[h^{-1}\ {\rm M}_{\odot}]) = 12.24^{+0.29}_{-0.40}$.

4.4.2 Large-scale Bias Method: Bias Evolution to Clustering Length

The corrected absolute linear bias of SMGs can be approximated as the large-scale bias, where $b_{\rm L} = b_{\rm sb} = 2.67 \pm 1.05$. We estimate the clustering length solely with the fixed $\gamma = 1.8$, as described in Section 3.5.2. We derive a clustering length of $r_{0,\rm SS,L,b} = 4.50 \pm 1.96\ h^{-1}$ Mpc, and the clustering length of SMGs with blending correction has been shown as the green circle in Fig. 4.3 on page 36.

The corrected DM halo mass of SMGs is $\log(M_{\rm halo,SMG}[h^{-1}\ {\rm M}_{\odot}]) = 11.90^{+0.61}_{-1.22}$.

<table>
<tr><td colspan="5">Assume $\gamma = 1.8$,</td></tr>
<tr><td rowspan="7">SMG</td><td></td><td>b</td><td>r_0 (h^{-1} Mpc)</td><td>$M_{\rm halo}$ (log h^{-1} M$_{\odot}$)</td></tr>
<tr><td colspan="4">Without blending bias correction,</td></tr>
<tr><td>Power Law Method</td><td>3.63 ± 1.45</td><td>6.46 ± 1.33</td><td>$12.46^{+0.52}_{-0.98}$</td></tr>
<tr><td colspan="4">With blending bias correction,</td></tr>
<tr><td>Power Law Method</td><td>2.67 ± 1.05</td><td>5.47 ± 1.12</td><td>$12.24^{0.29}_{-0.40}$</td></tr>
<tr><td>Large-scale Bias Method</td><td>2.67 ± 1.05</td><td>4.50 ± 1.96</td><td>$11.90^{+0.61}_{-1.22}$</td></tr>
</table>

Table 4.3: Results of clustering length, galaxy bias, and DM halo mass.

doi:10.6342/NTU201800137

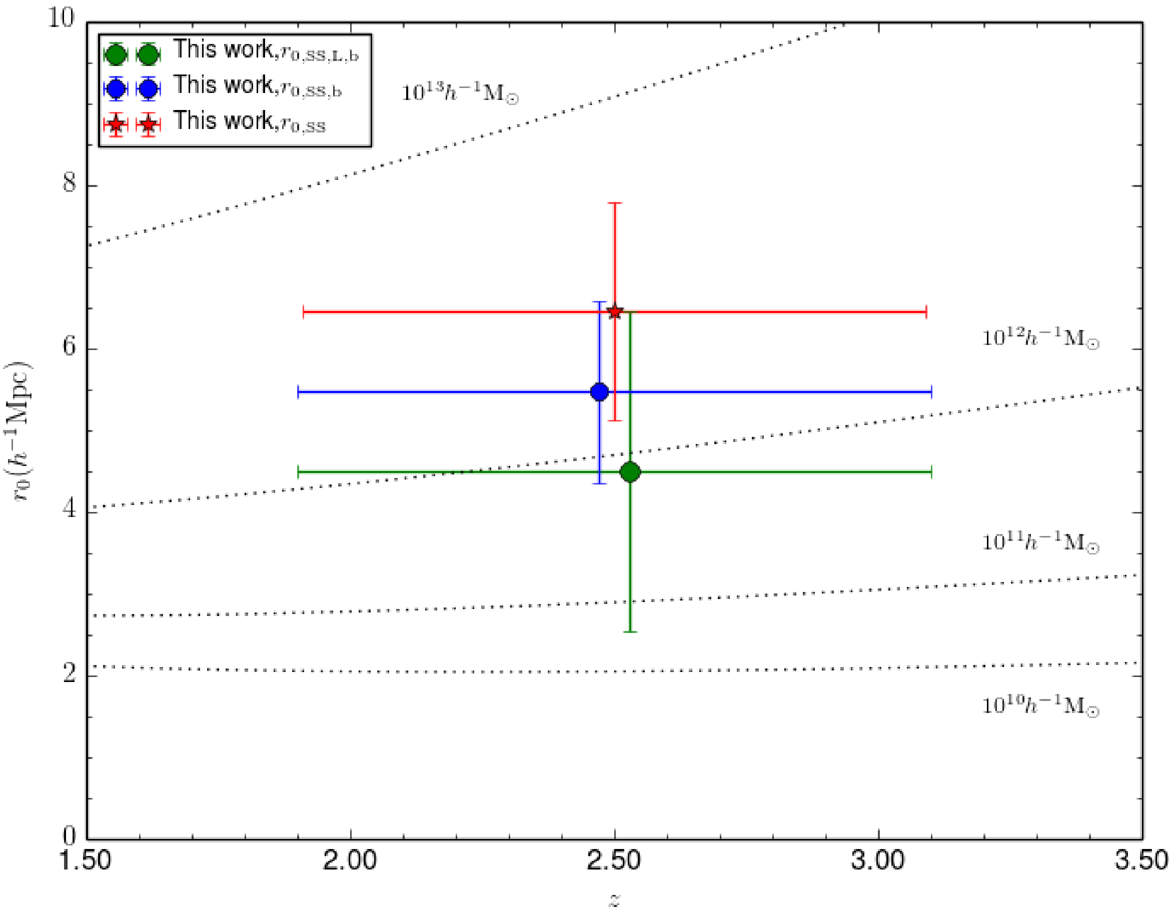

Figure 4.3: The clustering length r_0 as a function of redshift. This figure shows the linear perturbation prediction of the evolution of clustering length and DM halos at large-scale.
The z-positions of this work have been offset to exaggerate the difference.
Red star is the clustering length of SMGs without blending correction, $r_{0,\mathrm{SS}}$;
Blue diamond is the clustering length of SMGs with blending correction, $r_{0,\mathrm{SS,b}}$;
Green circle is the clustering length of SMGs computed by large-scale bias with blending effect correction,$r_{0,\mathrm{SS,L,b}}$. Since we do not know the exact blending effect, we maximize it according to Cowley et al. (2017) and estimate the smallest r_0 possible. The exact clustering length within $4-6\ h^{-1}$ Mpc.

doi:10.6342/NTU201800137

4.5 Clustering Result and Comparison to Previous Works

Note that we do not know the exact blending bias value so we apply a theoretical maximal blending correction, therefore the actual clustering lengths lie roughly between $4 - 6\ h^{-1}$ Mpc. We summarize the results in Table 4.3 and Fig. 4.3 on page 36. The redshift positions in Fig. 4.3 have been shifted to exaggerate the possible regions for clustering length. The two methods in Section 4.4.1 and 4.4.2 return similar results, which are consistent reasonably within 1σ confidence interval when compared to previous results, as shown in Fig. 4.4 on page 39. Recently Hickox et al. (2012) conducted projected cross-correlation measurement between radio-detected SMGs and IRAC galaxies in ECDFS, and they reported strong clustering result with $r_0 = 7.7^{+1.7}_{-2.3}\ h^{-1}$ Mpc and $b = 3.37 \pm 0.82$. However, our works actually show good agreement particularly with Wilkinson et al. (2017) ($r_0 = 4.1^{+2.1}_{-2.0}\ h^{-1}$ Mpc and $b = 2.18 \pm 0.97$), who used 365 SMGs in the much larger UKIDSS field (a sample size 3 times larger than ours). The studies here and Wilkinson et al. (2017) adopt similar methodology (they use the large-scale bias method to derive clustering length) and thereby strengthen the result of apparently weak clustering of SMGs. The weak clustering result implies the idea that SMGs reside in smaller halos, however it has been proposed in Chapman et al. (2009). Motivated by the presence of a large overdensity of SMGs and powerful star-forming galaxies, they suggested that SMGs obey complex bias that depends on large-scale environment and merger history, and that SMGs may reside in smaller halos than previously inferred from a linear bias model at large-scale. In that case, SMGs do not necessarily trace the most massive dark matter halos in the Universe.

The relatively weak clustering that we derive may be affected by the complex nature of SMG clustering which is redshift dependent (Wilkinson et al. 2017). Previous studies reported that low redshift SMGs tend to dilute the bias measurement, as well as the clustering length. Our study avoid this by excluding redshift information of SMGs; we use a log-normal redshift distribution model which peak at $z \sim 2$. However, our SMG samples do not necessarily follow the redshift distribution model, which results in the misinterpretation of derived clustering length from the model.

doi:10.6342/NTU201800137

Blending bias has significant impact on the galaxy bias. It boosts our derived $M_{\rm halo}$ to be 3 times larger. As suggested in Cowley et al. (2015), surveys with larger beams are subjected to a greater blending bias. For Hickox et al. (2012) and Weiß et al. (2009), their clustering measurements were carried out with the ECDFS LABOCA survey, which has a beam FWHM of $\sim 20''$. Similarly, SMGs in Williams et al. (2011) work were selected by utilizing the AzTEC/ASTE beam FWHM of $28''$. The clustering measurements in the previous literature are therefore subject to a larger correction than the value derived for the current SCUBA-2 surveys. It is likely that the correction for blending would bring previous studies into a better agreement with the clustering measurements presented here.

Previous studies have small sample sizes, which typically comprised more luminous (radio-identified) SMGs (e.g., Williams et al. 2011 study on $S_{870} \geq 8$ mJy Hickox et al. 2012 study on $S_{870} \geq 4$ mJy). In contrast, our sample of SMGs includes very faint sources (~ 2.0 mJy). Wilkinson et al. (2017) have presented that fainter SMGs without radio counterparts would dilute the clustering measurement and propose the idea that faint SMGs are less-clustered. Therefore, it is possible that previous clustering measurements were biased towards the brightest radio-selected SMGs, which could be a more luminous subset of the SMG population.

Investigating the possibility of clustering dependence on radio emission and S_{850} flux density further would require a much larger sample of SMGs. We leave this as a future improvement of this work.

In our analysis, SMGs lie in the DM halos similar to bright Lyman-break galaxies (LBGs), as shown in Fig. 4.4 on page 39. This may imply that SMGs will not descend into the most massive local elliptical galaxies as suggested in the literatures. However, our sample contains faint sources that possibly originated from low mass systems or very early epoch, so we cannot differentiate the two cases with the current data. Therefore, we cannot make a strong conclusion on the local descendant of SMGs.

doi:10.6342/NTU201800137

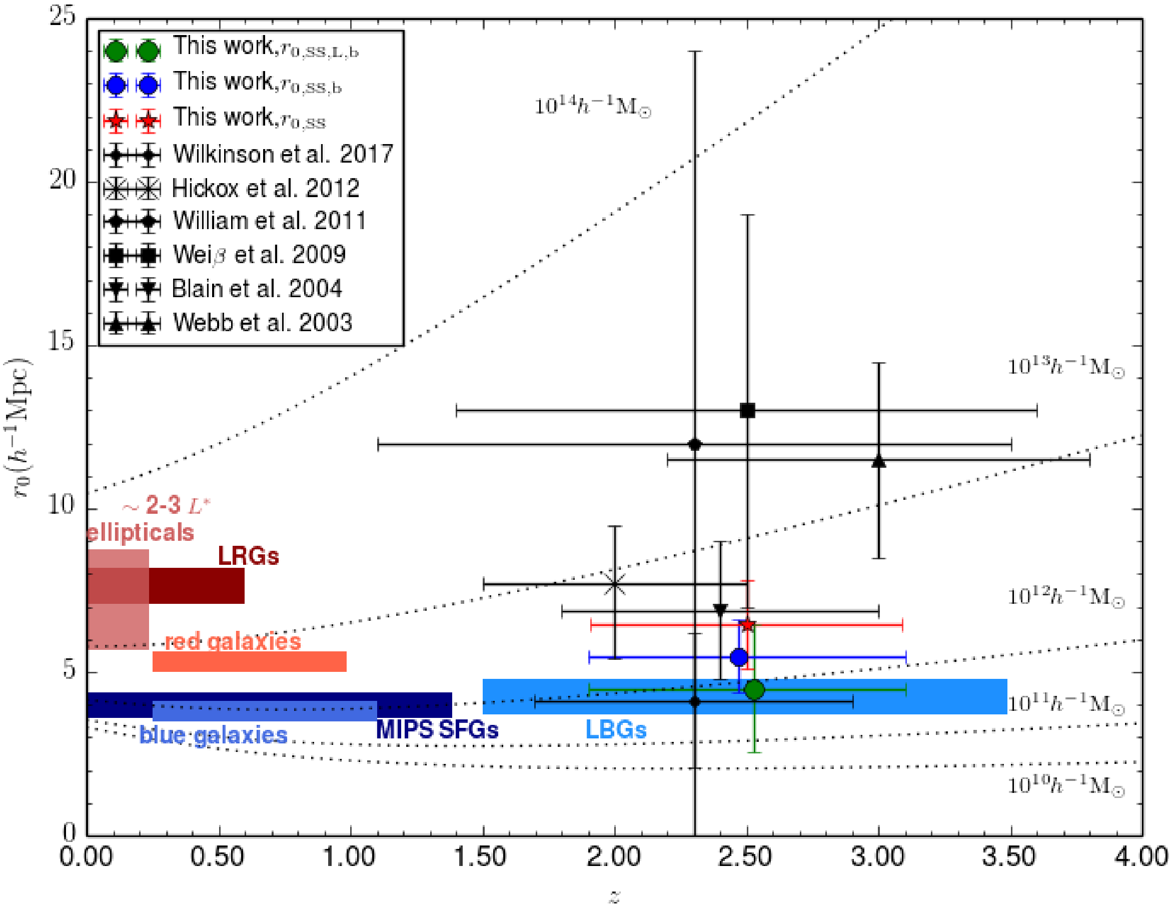

Figure 4.4: Comparison of this work to the literature studies. The black points are clustering results from previous studies: Webb et al. (2003); Blain et al. (2004); Weiß et al. (2009); Williams et al. (2011); Hickox et al. (2012); Wilkinson et al. (2017). The curves represent the predicted clustering strengths for DM halos of varying masses (labelled, in solar masses), produced using the formalism of Sheth et al. (2001). Colored regions are different galaxy populations illustrated in Hickox et al. (2012): LBGs at $1.5 < z < 3.5$ (Adelberger et al. 2005), Multiband Imaging Photometer for *Spitzer* (MIPS) 24-μm-selected star-forming galaxies (SFGs) at $0 < z < 1.4$ (Gilli et al. 2007), typical red and blue galaxies at $0.25 < z < 1$ from the AGN and Galaxy Evolution Survey (Hickox et al. 2009) and Deep Extragalactic Evolutionary Probe 2 (DEEP2; Coil et al. 2008) spectroscopic surveys, luminous red galaxies (LRGs) at $0 < z < 0.7$ (Wake et al. 2008) and low redshift elliptical galaxies with r-band luminosities in the range 1.5–3.5 L^*, derived from the luminosity dependence of clustering presented by Zehavi et al. (2011).

doi:10.6342/NTU201800137

4.6 Discrepancy and Improvement

Several questions arose during the course of our analysis. First, the use of flux-limited near-infrared galaxies cannot provide strong constraint on their hosting DM halo mass. K_s galaxies with a wide range of stellar mass entering the correlation mingles the estimated DM halo mass. Some of the bright or less massive galaxies may either enhance or reduce the bias measurement, providing different contributions to the bias. Therefore, a more reasonable way is to use a mass-limited sample for the analysis, where derived DM halo mass better reflects the population contribution from particular redshift with similar luminosity. With such a better characterized normal galaxy sample, we could have better constraints on the clustering properties of SMGs.

The other significant issue is the use of the large-scale relation in Section 3.5.2 in our work, which is obviously based on very small fields. The power law model for two-point correlation function is found to be valid for larger field surveys, typically with areas of several degree^2, where the large-scale linear perturbation dominates the mass growth. We calculate the correlation function on a small scale of $\sim 1\ h^{-1}$ Mpc, which is in the regime of nonlinear perturbation; our estimation of bias and DM halo mass is also made within the linear regime, which is not quite realistic, therefore here we actually need to consider the nonlinear effect here. Halo Occupation Model (HOD) simulations suggested that galaxies evolve into two-halo (different galaxies lie in different hosting DM halos) at linear large-scale, and gradually shift into one-halo (a host galaxy with several satellite galaxies in one DM halo) in the nonlinear small scale. Recall the CCF result (see Fig. 4.2 on page 32): the missing part between $8'' \leq \theta \leq 20''$ corresponds to a scale of ~ 100 kpc at $z = 2.5$, which is a possible region where density perturbation grows from linear into nonlinear regime. As a result, care must be taken to separate the result into both linear and nonlinear regime and to take the one-halo term in HOD modeling into account, i.e., the occupation number and the satellite composition. If the composite of observed bias at $\theta < 10''$ consists of contributions from both host and satellite galaxies, we expect that the host SMGs to have a smaller absolute bias, hence a smaller DM halo mass.

doi:10.6342/NTU201800137

國立臺灣大學 愛國・愛學・勵品・敦

Chapter 5

Conclusions

We perform a cross-correlation analysis to study the clustering properties of SMG in $1 < z < 3$. We use the extracted SMG samples from deep observation at 850 μm with SCUBA-2 in the GOODS fields. We cross-correlate the SMG samples with K_s-selected near-infrared galaxies as a tracer population, and try to infer the expected clustering length and halo mass of SMGs. Our main results are summarized as follows.

1. We find weaker clustering signal than those previously reported, with clustering strength $r_{0,\mathrm{SS,b}} = 5.47{\pm}1.12\, h^{-1}$ Mpc or $r_{0,\mathrm{SS,L,b}} = 4.50{\pm}1.96\, h^{-1}$ Mpc . However, within 1σ confidence interval, this is consistent with the result from the recent work of Wilkinson et al. (2017), who used the largest SMG sample sizes and survey area to date.

2. We analyze the redshift evolution of SMG clustering, derive DM halo mass, and compare them with previous measurements. The typical DM halo mass is found to be $M_\mathrm{halo} \sim 7.9 - 17.4 \times 10^{11}\ M_\odot$. We find no evidence that SMGs may descend into local massive elliptical galaxies as previously suggested in the literatures.

This work excludes the SMGs redshift information and uses a redshift distribution model when deriving clustering properties. We expect the result can be better constrained if we include the accurate SMG redshift information. Another way to improve the result is to take account the full redshift PDF for both SMGs and tracer populations. With sufficient

doi:10.6342/NTU201800137

redshift information we can apply the projected cross-correlation measurement which has a smaller statistical error to obtain reliable result.

doi:10.6342/NTU201800137

Bibliography

K. L. Adelberger, C. C. Steidel, M. Pettini, A. E. Shapley, N. A. Reddy, and D. K. Erb. The Spatial Clustering of Star-forming Galaxies at Redshifts $1.4 \lesssim z \lesssim 3.5$. *Astrophys. J.*, 619:697, 2005.

D. M. Alexander, F. E. Bauer, S. C. Chapman, I. Smail, A. W. Blain, W. N. Brandt, and R. J. Ivison. The X-Ray Spectral Properties of SCUBA Galaxies. *Astrophys. J.*, 632 (2):736–750, 2005.

D. M. Alexander, W. N. Brandt, I. Smail, A. M. Swinbank, F. E. Bauer, A. W. Blain, S. C. Chapman, K. E. K. Coppin, R. J. Ivison, and K. Menendez-Delmestre. Weighing the black holes in Z˜2 submillimeter-emitting galaxies hosting active galactic nuclei. *Astron. J.*, 135(5):1968–1981, 2008.

S. P. Allanson, M. J. Hudson, R. J. Smith, and J. R. Lucey. The star formation histories of red-sequence galaxies, mass-to-light ratios and the fundamental plane. *Astrophys. J.*, 702(2):1275–1296, 2009.

C. Almeida, C. M. Baugh, and C. G. Lacey. Modelling the dusty universe - II. The clustering of submillimetre-selected galaxies. *Mon. Not. R. Astron. Soc.*, 417(3):2057–2071, 2011.

R. J. Assef, C. S. Kochanek, M. L. Ashby, M. Brodwin, M. J. Brown, R. Cool, W. Forman, A. H. Gonzalez, R. C. Hickox, B. T. Jannuzi, C. Jones, E. Le Floc'h, J. Moustakas, S. S. Murray, and D. Stern. The mid-IR-and X-ray-selected QSO luminosity function. *Astrophys. J.*, 728(1), 2011.

doi:10.6342/NTU201800137

J. Bardeen, J. R. Bond, N. Kaiser, and A. S. Szalay. The statistics of peaks of Gaussian random fields. *Astrophys. J.*, 304:15–61, 1986.

A. J. Barger, L. L. Cowie, D. B. Sanders, E. Fulton, Y. Taniguchi, Y. Sato, K. Kawara, and H. Okuda. Submillimetre-wavelength detection of dusty star-forming galaxies at high redshift. *Nature*, 394(6690):248–251, 1998.

V. N. Bennert, T. Treu, J. H. Woo, M. A. Malkan, A. Le Bris, M. W. Auger, S. Gallagher, and R. D. Blandford. Cosmic evolution of black holes and spheroids. IV. the M BH-L sph relation. *Astrophys. J.*, 708(2):1507–1527, 2010.

A. W. Blain, I. Smail, R. J. Ivison, J. P. Kneib, and D. T. Frayer. Submillimeter galaxies. *Phys. Rep.*, 369(2):111–176, 2002.

A. W. Blain, S. C. Chapman, I. Smail, and R. Ivison. Clustering of Submillimeter□selected Galaxies. *Astrophys. J.*, 611(2):725–731, 2004.

C. Blake, A. Pope, D. Scott, and B. Mobasher. On the cross-correlation of sub-mm sources and optically selected galaxies. *Mon. Not. R. Astron. Soc.*, 368(2):732–740, 2006.

C. Borys, S. Chapman, M. Halpern, and D. Scott. The Hubble Deep Field North SCUBA Super-map - I. Submillimetre maps, sources and number counts. *Mon. Not. R. Astron. Soc.*, 344(September):385–398, 2003.

D. Brisbin, O. Miettinen, M. Aravena, V. Smolčić, I. Delvecchio, C. Jiang, B. Magnelli, M. Albrecht, A. M. Arancibia, H. Aussel, N. Baran, F. Bertoldi, M. Béthermin, P. Capak, C. M. Casey, F. Civano, C. C. Hayward, O. Ilbert, A. Karim, O. L. Fevre, S. Marchesi, H. J. McCracken, F. Navarrete, M. Novak, D. Riechers, N. Padilla, M. Salvato, K. Scott, E. Schinnerer, K. Sheth, and L. Tasca. An ALMA survey of submillimeter galaxies in the COSMOS field: Multiwavelength counterparts and redshift distribution. *Astron. Astrophys.*, 608:A15, 2017. ISSN 14320746.

F. J. Carrera, M. J. Page, J. A. Stevens, R. J. Ivison, T. Dwelly, J. Ebrero, and S. Falocco. A strongly star-forming group: Three massive galaxies associated with a quasi-stellar object. *Mon. Not. R. Astron. Soc.*, 413(4):2791–2807, 2011.

doi:10.6342/NTU201800137

S. Carroll, W. Press, and T. E.L. The Cosmological Constant. *Annu. Rev. Astron. Astrophys.*, 30:499–542, 1992.

S. C. Chapman, a. W. Blain, R. J. Ivison, and I. R. Smail. A median redshift of 2.4 for galaxies bright at submillimetre wavelengths. *Nature*, 422(6933):695–8, 2003.

S. C. Chapman, A. W. Blain, I. Smail, and R. J. Ivison. A Redshift Survey of the Submillimeter Galaxy Population. *Astrophys. J.*, 622(2):772–796, 2005.

S. C. Chapman, A. Blain, R. Ibata, R. J. Ivison, I. Smail, and G. Morrison. Do submillimeter galaxies really trace the most massive dark-matter halos? Discovery of a high-z cluster in a highly active phase of evolution. *Astrophys. J.*, 691(1):560–568, 2009.

C.-C. Chen, I. Smail, R. J. Ivison, V. Arumugam, O. Almaini, C. J. Conselice, J. E. Geach, W. G. Hartley, C.-J. Ma, A. Mortlock, C. Simpson, J. M. Simpson, A. M. Swinbank, I. Aretxaga, A. Blain, S. C. Chapman, J. S. Dunlop, D. Farrah, M. Halpern, M. J. Michałowski, P. van der Werf, A. Wilkinson, and J. A. Zavala. The SCUBA-2 Cosmology Legacy Survey: Multi-wavelengths counterparts to 10$ˆ3$ submillimeter galaxies in the UKIDSS-UDS field. *Astrophys. J.*, 82, 2016.

A. L. Coil, J. A. Newman, D. Croton, M. C. Cooper, M. Davis, S. M. Faber, B. F. Gerke, D. C. Koo, N. Padmanabhan, R. H. Wechsler, and B. J. Weiner. The DEEP2 Galaxy Redshift Survey: Color and Luminosity Dependence of Galaxy Clustering at z ˜ 1. *Astrophys. J.*, 672(1):153–176, 2008.

L. L. Cowie, A. J. Barger, L.-Y. Hsu, C.-C. Chen, F. N. Owen, and W.-H. Wang. A Submillimeter Perspective on the GOODS Fields (SUPER GOODS) - I. An Ultradeep SCUBA-2 Survey of the GOODS-N. *Astrophys. J.*, 837(2):139, 2017.

W. I. Cowley, C. G. Lacey, C. M. Baugh, and S. Cole. Simulated observations of submillimetre galaxies: The impact of single-dish resolution and field variance. *Mon. Not. R. Astron. Soc.*, 446(2):1784–1798, 2015.

W. I. Cowley, C. G. Lacey, C. M. Baugh, S. Cole, and A. Wilkinson. Blending bias impacts

doi:10.6342/NTU201800137

the host halo masses derived from a cross-correlation analysis of bright sub-millimetre galaxies. *Mon. Not. R. Astron. Soc.*, 469(Aug):3396–3404, 2017.

S. M. Croom, D. Schade, B. J. Boyle, T. Shanks, L. Miller, and R. J. Smith. Gemini Imaging of QSO Host Galaxies at z □ 2. *Astrophys. J.*, 606(1):126–138, 2004.

R. Davé, K. Finlator, B. D. Oppenheimer, M. Fardal, N. Katz, D. Kereš, and D. H. Weinberg. The nature of submillimetre galaxies in cosmological hydrodynamic simulations. *Mon. Not. R. Astron. Soc.*, 404(3):1355–1368, 2010.

R. Decarli, R. Falomo, A. Treves, M. Labita, J. K. Kotilainen, and R. Scarpa. The quasar MBH-Mhost relation through cosmic time - II. Evidence for evolution from z = 3 to the present age. *Mon. Not. R. Astron. Soc.*, 402(4):2453–2461, 2010.

A. Durkalec, O. Le Fèvre, A. Pollo, S. de la Torre, P. Cassata, B. Garilli, V. Le Brun, B. C. Lemaux, D. Maccagni, L. Pentericci, L. A. M. Tasca, R. Thomas, E. Vanzella, G. Zamorani, E. Zucca, R. Amorín, S. Bardelli, L. P. Cassarà, M. Castellano, A. Cimatti, O. Cucciati, A. Fontana, M. Giavalisco, A. Grazian, N. P. Hathi, O. Ilbert, S. Paltani, B. Ribeiro, D. Schaerer, M. Scodeggio, V. Sommariva, M. Talia, L. Tresse, D. Vergani, P. Capak, S. Charlot, T. Contini, J. G. Cuby, J. Dunlop, S. Fotopoulou, A. Koekemoer, C. López-Sanjuan, Y. Mellier, J. Pforr, M. Salvato, N. Scoville, Y. Taniguchi, and P. W. Wang. Evolution of clustering length, large-scale bias, and host halo mass at $2 < z < 5$ in the VIMOS Ultra Deep Survey (VUDS). *Astron. Astrophys.*, 583:A128, 2015.

S. Eales, S. Lilly, W. Gear, L. Dunne, J. R. Bond, F. Hammer, O. Le Fèvre, and D. Crampton. The Canada-UK Deep Submillimeter Survey: First Submillimeter Images, the Source Counts, and Resolution of the Background. *Astrophys. J.*, 515(2):518–524, 1999.

O. Fakhouri, C. P. Ma, and M. Boylan-Kolchin. The merger rates and mass assembly histories of dark matter haloes in the two Millennium simulations. *Mon. Not. R. Astron. Soc.*, 406(4):2267–2278, 2010.

doi:10.6342/NTU201800137

S. Fine, S. M. Croom, J. Bland-Hawthorn, K. A. Pimbblet, N. P. Ross, D. P. Schneider, and T. Shanks. The C iv linewidth distribution for quasars and its implications for broad-line region dynamics and virial mass estimation. *Mon. Not. R. Astron. Soc.*, 409(2): 591–610, 2010.

M. Giavalisco, H. C. Ferguson, A. M. Koekemoer, M. Dickinson, D. M. Alexander, F. E. Bauer, J. Bergeron, C. Biagetti, W. N. Brandt, S. Casertano, C. Cesarsky, E. Chatzichristou, C. Conselice, S. Cristiani, L. D. Costa, T. Dahlen, D. D. Mello, P. Eisenhardt, T. Erben, S. M. Fall, C. Fassnacht, R. Fosbury, A. Fruchter, J. P. Gardner, N. Grogin, R. N. Hook, A. E. Hornschemeier, R. Idzi, S. Jogee, C. Kretchmer, V. Laidler, K. S. Lee, M. Livio, R. Lucas, P. Madau, B. Mobasher, L. A. Moustakas, M. Nonino, P. Padovani, C. Papovich, Y. Park, S. Ravindranath, A. Renzini, M. Richardson, A. Riess, P. Rosati, M. Schirmer, E. Schreier, R. S. Somerville, H. Spinrad, D. Stern, M. Stiavelli, and L. Strolger. The Great Observatories Origins Deep Survey: Initial Results from Optical and Near-Infrared Imaging. *Astrophys. J.*, 600(2):L93–L98, 2004.

R. Gilli, E. Daddi, R. Chary, M. Dickinson, D. Elbaz, M. Giavalisco, M. Kitzbichler, D. Stern, and E. Vanzella. The spatial clustering of mid-IR selected star forming galaxies at z ˜ 1 in the GOODS fields. *Astron. Astrophys.*, 475:83, 2007.

T. R. Greve, F. Bertoldi, I. Smail, R. Neri, S. C. Chapman, A. W. Blain, R. J. Ivison, R. Genzel, A. Omont, P. Cox, L. Tacconi, and J. P. Kneib. An interferometric CO survey of luminous submillimetre galaxies. *Mon. Not. R. Astron. Soc.*, 359(3):1165–1183, 2005.

J. E. Groth and P. J. E. Peebles. Statistical analysis of catalogs of extragalactic objects. VII. Two- and three-point correlation functions for the high-resolution Shane-Wirtanen Catalog of Galaxies. *Astrophys. J.*, 217(10):385–405, 1977.

L. J. Hainline, A. W. Blain, I. Smail, D. M. Alexander, L. Armus, S. C. Chapman, and R. J. Ivison. The stellar mass content of submillimeter-selected galaxies. *Astrophys. J.*, 740(2), 2011.

doi:10.6342/NTU201800137

R. C. Hickox, C. Jones, W. R. Forman, S. S. Murray, C. S. Kochanek, D. Eisenstein, B. T. Jannuzi, A. Dey, M. J. I. Brown, D. Stern, P. R. Eisenhardt, V. Gorjian, M. Brodwin, R. Narayan, R. J. Cool, A. Kenter, N. Caldwell, and M. E. Anderson. Host galaxies, clustering, Eddington ratios, and evolution of radio, X-ray, and infrared-selected AGNs. *Astrophys. J.*, 696(1):891–919, 2009.

R. C. Hickox, A. D. Myers, M. Brodwin, D. M. Alexander, W. R. Forman, C. Jones, S. S. Murray, M. J. Brown, R. J. Cool, C. S. Kochanek, A. Dey, B. T. Jannuzi, D. Eisenstein, R. J. Assef, P. R. Eisenhardt, V. Gorjian, D. Stern, E. Le Floc'H, N. Caldwell, A. D. Goulding, and J. R. Mullaney. Clustering of obscured and unobscured quasars in the Boötes field: Placing rapidly growing black holes in the cosmic web. *Astrophys. J.*, 731 (2), 2011.

R. C. Hickox, J. L. Wardlow, I. Smail, A. D. Myers, D. M. Alexander, A. M. Swinbank, A. L. Danielson, J. P. Stott, S. C. Chapman, K. E. Coppin, J. S. Dunlop, E. Gawiser, D. Lutz, P. van der Werf, and A. Weiß. The LABOCA survey of the Extended Chandra Deep Field-South: Clustering of submillimetre galaxies. *Mon. Not. R. Astron. Soc.*, 421 (1):284–295, 2012.

J. A. Hodge, A. Karim, I. Smail, A. M. Swinbank, F. Walter, A. D. Biggs, R. J. Ivison, A. Weiss, D. M. Alexander, F. Bertoldi, W. N. Brandt, S. C. Chapman, K. E. K. Coppin, P. Cox, A. L. R. Danielson, H. Dannerbauer, C. De Breuck, R. Decarli, A. C. Edge, T. R. Greve, K. K. Knudsen, K. M. Menten, H. W. Rix, E. Schinnerer, J. M. Simpson, J. L. Wardlow, and P. Van Der Werf. An alma survey of submillimeter galaxies in the extended chandra deep field south: Source catalog and multiplicity. *Astrophys. J.*, 768 (1), 2013.

B. C. Hsieh, W. H. Wang, C. C. Hsieh, L. Lin, H. Yan, J. Lim, and P. T. P. Ho. The taiwan ecdfs near-infrared survey: Ultra-deep J and K S imaging in the extended chandra deep field-south. *Astrophys. Journal, Suppl. Ser.*, 203(2), 2012.

L.-T. Hsu, M. Salvato, K. Nandra, M. Brusa, R. Bender, J. Buchner, J. L. Donley, D. D. Kocevski, Y. Guo, N. P. Hathi, C. Rangel, S. P. Willner, M. Brightman, A. Georgakakis,

doi:10.6342/NTU201800137

T. Budavári, A. S. Szalay, M. L. N. Ashby, G. Barro, T. Dahlen, S. M. Faber, H. C. Ferguson, A. Galametz, A. Grazian, N. A. Grogin, K.-H. Huang, A. M. Koekemoer, R. A. Lucas, E. McGrath, B. Mobasher, M. Peth, D. J. Rosario, and J. R. Trump. Candels/Goods-S, Cdfs, and Ecdfs: Photometric Redshifts for Normal and X-Ray-Detected Galaxies. *Astrophys. J.*, 796(1):60, 2014.

D. Hughes, S. Serjeant, J. Dunlop, M. Rowan-Robinson, A. Blain, R. G. Mann, R. Ivison, J. Peacock, A. Efstathiou, W. Gear, S. Oliver, A. Lawrence, M. Longair, P. Goldschmidt, and T. Jenness. Unveiling Dust-enshrouded Star Formation in the Early Universe: a Sub-mm Survey of the Hubble Deep Field. *Nature*, 394:241, 1998.

T. Ichikawa, R. Suzuki, C. Tokoku, Y. K. Uchimoto, M. Konishi, T. Yoshikawa, M. Kajisawa, M. Ouchi, T. Hamana, M. Akiyama, T. Nishimura, K. Omata, I. Tanaka, and T. Yamada. MOIRCS Deep Survey. II. Clustering Properties of K-Band Selected Galaxies in GOODS-North Region. *Publ. Astron. Soc. Japan*, 59:1081, 2007.

R. J. Ivison, P. P. Papadopoulos, I. Smail, T. R. Greve, A. P. Thomson, E. M. Xilouris, and S. C. Chapman. Tracing the molecular gas in distant submillimetre galaxies via CO(1-0) imaging with the Expanded Very Large Array. *Mon. Not. R. Astron. Soc.*, 412 (3):1913–1925, 2011.

N. Kaiser. On the spatial correlations of Abell clusters. *Astrophys. J. Lett.*, 284:L9–L12, 1984.

A. Karim, A. M. Swinbank, J. A. Hodge, I. R. Smail, F. Walter, A. D. Biggs, J. M. Simpson, A. L. Danielson, D. M. Alexander, F. Bertoldi, C. de Breuck, S. C. Chapman, K. E. Coppin, H. Dannerbauer, A. C. Edge, T. R. Greve, R. J. Ivison, K. K. Knudsen, K. M. Menten, E. Schinnerer, J. L. Wardlow, A. Weiß, and P. van der Werf. An alma survey of submillimetre galaxies in the extended chandra deep field south: High-Resolution 870 μm source counts. *Mon. Not. R. Astron. Soc.*, 432(1):2–9, 2013.

B. C. Kelly, M. Vestergaard, X. Fan, P. Hopkins, L. Hernquist, and A. Siemiginowska. Constraints on black hole growth, quasar lifetimes, and Eddington ratio distributions

doi:10.6342/NTU201800137

from the SDSS broad-line quasar black hole mass function. *Astrophys. J.*, 719(2):1315–1334, 2010.

J. A. Kollmeier, C. A. Onken, C. S. Kochanek, A. Gould, D. H. Weinberg, M. Dietrich, R. Cool, A. Dey, D. J. Eisenstein, B. T. Jannuzi, E. Le Floc'h, and D. Stern. Black Hole Masses and Eddington Ratios at $0.3 < z < 4$. *Astrophys. J.*, 648(1):128–139, 2006.

J. K. Kotilainen, R. Falomo, R. Decarli, A. Treves, M. Uslenghi, and R. Scarpa. The properties of quasar hosts at the peak of the quasar activity. *Astrophys. J.*, 703(2):1663–1671, 2009.

C. G. Lacey and S. Cole. Merger rates in hierarchical models of galaxy formation. *Mon. Not. R. Astron. Soc.*, 262:627–649, 1993.

S. D. Landy and A. S. Szalay. Bias and variance of angular correlation functions. *Astrophys. J.*, 412:64, 1993.

T. R. Lauer, S. Tremaine, D. Richstone, and S. M. Faber. Selection Bias in Observing the Cosmological Evolution of the M•□σ and M•□ L Relationships. *Astrophys. J.*, 670(1):249–260, 2007.

R. R. Lindner, A. J. Baker, A. Omont, A. Beelen, F. N. Owen, F. Bertoldi, H. Dole, N. Fiolet, A. I. Harris, R. J. Ivison, C. J. Lonsdale, D. Lutz, and M. Polletta. A deep 1.2mm map of the lockman hole north field. *Astrophys. J.*, 737(2), 2011.

S. N. Lindsay, M. J. Jarvis, and K. McAlpine. Evolution in the bias of faint radio sources to z ˜ 2.2. *Mon. Not. R. Astron. Soc.*, 440(3):2322–2332, 2014.

A. Marconi, D. J. Axon, R. Maiolino, T. Nagao, G. Pastorini, P. Pietrini, A. Robinson, and G. Torricelli. The Effect of Radiation Pressure on Virial Black Hole Mass Estimates and the Case of Narrow□Line Seyfert 1 Galaxies. *Astrophys. J.*, 678(2):693–700, 2008.

A. Merloni, A. Bongiorno, M. Bolzonella, M. Brusa, F. Civano, A. Comastri, M. Elvis, F. Fiore, R. Gilli, H. Hao, K. Jahnke, A. M. Koekemoer, E. Lusso, V. Mainieri, M. Mignoli, T. Miyaji, A. Renzini, M. Salvato, J. Silverman, J. Trump, C. Vignali,

doi:10.6342/NTU201800137

G. Zamorani, P. Capak, S. J. Lilly, D. Sanders, Y. Taniguchi, S. Bardelli, C. M. Carollo, K. Caputi, T. Contini, G. Coppa, O. Cucciati, S. De La Torre, L. De Ravel, P. Franzetti, B. Garilli, G. Hasinger, C. Impey, A. Iovino, K. Iwasawa, P. Kampczyk, J. P. Kneib, C. Knobel, K. Kova, F. Lamareille, J. F. Le Borgne, V. Le Brun, O. Le Fèvre, C. Maier, R. Pello, Y. Peng, E. P. Montero, E. Ricciardelli, M. Scodeggio, M. Tanaka, L. A. Tasca, L. Tresse, D. Vergani, and E. Zucca. On the cosmic evolution of the scaling relations between black holes and their host galaxies: Broad-line active galactic nuclei in the zCosmos survey. *Astrophys. J.*, 708(1):137–157, 2010.

A. D. Myers, R. J. Brunner, G. T. Richards, R. C. Nichol, D. P. Schneider, D. E. Vanden Berk, R. Scranton, A. G. Gray, and J. Brinkmann. First Measurement of the Clustering Evolution of Photometrically Classified Quasars. *Astrophys. J.*, 638:622–634, 2006.

A. D. Myers, R. J. Brunner, R. C. Nichol, G. T. Richards, D. P. Schneider, and N. a. Bahcall. Clustering Analyses of 300,000 Photometrically Classified Quasars. I. Luminosity and Redshift Evolution in Quasar Bias. *Astrophys. J.*, 658:85–98, 2007.

A. D. Myers, M. White, and N. M. Ball. Incorporating photometric redshift probability density information into real-space clustering measurements. *Mon. Not. R. Astron. Soc.*, 399(4):2279–2287, 2009.

H. Netzer and P. Marziani. the Effect of Radiation Pressure on Emission-Line Profiles and Black Hole Mass Determination in Active Galactic Nuclei. *Astrophys. J.*, 724(1): 318–328, 2010.

R. A. Overzier, H. J. A. Röttgering, R. B. Rengelink, and R. J. Wilman. The spatial clustering of radio sources in NVSS and FIRST; implications for galaxy clustering evolution. *Astron. Astrophys.*, 405:53, 2003.

P. Peebles. *The large-scale structure of the universe*. Princeton University Press, Princeton, N.J., 1980.

P. Peebles. *Principles of Physical Cosmology*. Princeton University Press, Princeton, N.J., 1993.

doi:10.6342/NTU201800137

B. M. Peterson, L. Ferrarese, K. M. Gilbert, S. Kaspi, M. A. Malkan, D. Maoz, D. Merritt, H. Netzer, C. A. Onken, R. W. Pogge, M. Vestergaard, and A. Wandel. Central Masses and Broad-Line Region Sizes of Active Galactic Nuclei. II. A Homogeneous Analysis of a Large Reverberation-Mapping Database. *Astrophys. J.*, 613(2):682–699, 2004.

A. Pope, R.-R. Chary, D. M. Alexander, L. Armus, M. Dickinson, D. Elbaz, D. Frayer, D. Scott, and H. Teplitz. Mid-Infrared Spectral Diagnosis of Submillimeter Galaxies. *Astrophys. J.*, 675(2):1171–1193, 2008.

R. Quadri, P. van Dokkum, E. Gawiser, M. Franx, D. Marchesini, P. Lira, G. Rudnick, D. Herrera, J. Maza, M. Kriek, I. Labbé, and H. Francke. Clustering of K-selected Galaxies at $2 < z < 3.5$: Evidence for a Color-Density Relation. *Astrophys. J.*, 654:138, 2007.

D. A. Rafferty, W. N. Brandt, D. M. Alexander, Y. Q. Xue, F. E. Bauer, B. D. Lehmer, B. Luo, and C. Papovich. SUPERMASSIVE BLACK HOLE GROWTH IN STARBURST GALAXIES OVER COSMIC TIME: CONSTRAINTS FROM THE DEEPEST CHANDRA FIELDS. *Astrophys. J.*, 742(1):3, 2011.

G. T. Richards, M. A. Strauss, X. Fan, P. B. Hall, S. Jester, D. P. Schneider, D. E. Vanden Berk, C. Stoughton, S. F. Anderson, R. J. Brunner, J. Gray, J. E. Gunn, Ž. Ivezić, M. K. Kirkland, G. R. Knapp, J. Loveday, A. Meiksin, A. Pope, A. S. Szalay, A. R. Thakar, B. Yanny, D. G. York, J. C. Barentine, H. J. Brewington, J. Brinkmann, M. Fukugita, M. Harvanek, S. M. Kent, S. J. Kleinman, J. Krzesiński, D. C. Long, R. H. Lupton, T. Nash, E. H. Neilsen, A. Nitta, D. J. Schlegel, and S. A. Snedden. The Sloan Digital Sky Survey Quasar Survey: Quasar Luminosity Function from Data Release 3. *Astrophys. J. Lett.*, 131:2766, 2006.

N. Roche and S. A. Eales. The angular correlation function and hierarchical moments of ˜70,000 faint galaxies to R=23.5. *Mon. Not. R. Astron. Soc*, 307(December):703–721, 1999.

S. E. Scott, M. J. Fox, J. S. Dunlop, S. Serjeant, J. A. Peacock, R. J. Ivison, S. Oliver,

doi:10.6342/NTU201800137

R. G. Mann, A. Lawrence, A. Efstathiou, M. Rowan-Robinson, D. H. Hughes, E. N. Archibald, A. Blain, and M. Longair. The SCUBA 8-mJy survey - I. Submillimetre maps, sources and number counts. *Mon. Not. R. Astron. Soc.*, 331(4):817–838, 2002.

Y. Shen and B. C. Kelly. The impact of the uncertainty in single-epoch virial black hole mass estimates on the observed evolution of the black hole-bulge scaling relations. *Astrophys. J.*, 713(1):41–45, 2010.

Y. Shen, J. E. Greene, M. A. Strauss, G. T. Richards, and D. P. Schneider. Biases in Virial Black Hole Masses: An SDSS Perspective. *Astrophys. J.*, 680(1):169–190, 2008.

R. K. Sheth, H. J. Mo, and G. Tormen. Ellipsoidal collapse and an improved model for the number and spatial distribution of dark matter haloes. *Mon. Not. R. Astron. Soc.*, 323(1):1–12, 2001.

J. M. Simpson, A. M. Swinbank, I. Smail, D. M. Alexander, W. N. Brandt, F. Bertoldi, C. De Breuck, S. C. Chapman, K. E. K. Coppin, E. Da Cunha, A. L. R. Danielson, H. Dannerbauer, T. R. Greve, J. A. Hodge, R. J. Ivison, A. Karim, K. K. Knudsen, B. M. Poggianti, E. Schinnerer, A. P. Thomson, F. Walter, J. L. Wardlow, A. Weiß, and P. P. Van Der Werf. An alma survey of submillimeter galaxies in the extended Chandra deep field south: The redshift distribution and evolution of submillimeter galaxies. *Astrophys. J.*, 788(2), 2014.

I. Smail, R. J. Ivison, and A. W. Blain. A Deep Submillimeter Survey of Lensing Clusters: A New Window on Galaxy Formation and Evolution. *Astrophys. J.*, 490(1):L5–L8, 1997.

R. E. Smith, J. A. Peacock, A. Jenkins, S. D. White, C. S. Frenk, F. R. Pearce, P. A. Thomas, G. Efstathiou, and H. M. Couchman. Stable clustering, the halo model and non-linear cosmological power spectra. *Mon. Not. R. Astron. Soc.*, 341(4):1311–1332, 2003.

V. Smolčić, M. Aravena, F. Navarrete, E. Schinnerer, D. A. Riechers, F. Bertoldi, C. Feruglio, A. Finoguenov, M. Salvato, M. Sargent, H. J. McCracken, M. Albrecht,

doi:10.6342/NTU201800137

A. Karim, P. Capak, C. L. Carilli, N. Cappelluti, M. Elvis, O. Ilbert, J. Kartaltepe, S. Lilly, D. Sanders, K. Sheth, N. Z. Scoville, and Y. Taniguchi. Millimeter imaging of submillimeter galaxies in the COSMOS field: redshift distribution. *Astron. Astrophys.*, 548:A4, 2012.

A. M. Swinbank, S. C. Chapman, I. Smail, C. Lindner, C. Borys, A. W. Blain, R. J. Ivison, and G. F. Lewis. The link between submillimetre galaxies and luminous ellipticals: Near-infrared IFU spectroscopy of submillimetre galaxies. *Mon. Not. R. Astron. Soc.*, 371(1):465–476, 2006.

L. J. Tacconi, R. Neri, S. C. Chapman, R. Genzel, I. Smail, R. J. Ivison, F. Bertoldi, A. Blain, P. Cox, T. Greve, and A. Omont. High□Resolution Millimeter Imaging of Submillimeter Galaxies. *Astrophys. J.*, 640(1):228–240, 2006.

L. J. Tacconi, R. Genzel, I. Smail, R. Neri, S. C. Chapman, R. J. Ivison, A. Blain, P. Cox, A. Omont, F. Bertoldi, T. Greve, N. M. Förster Schreiber, S. Genel, D. Lutz, a. M. Swinbank, a. E. Shapley, D. K. Erb, A. Cimatti, E. Daddi, and a. J. Baker. Submillimeter Galaxies at z ˜ 2: Evidence for Major Mergers and Constraints on Lifetimes, IMF, and CO-H2 Conversion Factor. *Astrophys. J.*, 680(1):246–262, 2008.

M. Vestergaard. Determining Central Black Hole Masses in Distant Active Galaxies. *Astrophys. J.*, 571(2):733–752, 2002.

M. Vestergaard and B. M. Peterson. Determining Central Black Hole Masses in Distant Active Galaxies and Quasars. II. Improved Optical and UV Scaling Relationships. *Astrophys. J.*, 641(2):689–709, 2006.

D. A. Wake, S. M. Croom, E. M. Sadler, and H. M. Johnston. The clustering of radio galaxies at $z = 0.55$ from the 2SLAQ LRG survey. *Mon. Not. R. Astron. Soc.*, 391(4): 1674–1684, 2008.

W. H. Wang, L. L. Cowie, A. J. Barger, R. C. Keenan, and H. C. Ting. Ultradeep KS imaging in the goods-N. *Astrophys. Journal, Suppl. Ser.*, 187(1):251–271, 2010.

doi:10.6342/NTU201800137

J. L. Wardlow, I. Smail, K. E. K. Coppin, D. M. Alexander, W. N. Brandt, A. L. R. Danielson, B. Luo, A. M. Swinbank, F. Walter, A. Weiss, Y. Q. Xue, S. Zibetti, F. Bertoldi, A. D. Biggs, S. C. Chapman, H. Dannerbauer, J. S. Dunlop, E. Gawiser, R. J. Ivison, K. K. Knudsen, A. Kovacs, C. G. Lacey, K. M. Menten, N. Padilla, H. W. Rix, and P. P. van der Werf. The LABOCA survey of the Extended Chandra Deep Field South: A photometric redshift survey of submillimetre galaxies. *Mon. Not. R. Astron. Soc.*, 23 (June):31, 2011.

T. M. Webb, S. Eales, S. Foucaud, S. J. Lilly, H. McCracken, K. Adelberger, C. Steidel, A. Shapley, D. L. Clements, L. Dunne, O. Le Fevre, M. Brodwin, and W. Gear. The Canada–United Kingdom Deep Submillimeter Survey. V. The Submillimeter Properties of Lyman Break Galaxies. *Astrophys. J.*, 582(1):6–16, 2003.

A. Weiß, A. Kovács, K. Coppin, T. R. Greve, F. Walter, I. Smail, J. S. Dunlop, K. K. Knudsen, D. M. Alexander, F. Bertoldi, W. N. Brandt, S. C. Chapman, P. Cox, H. Dannerbauer, C. De Breuck, E. Gawiser, R. J. Ivison, D. Lutz, K. M. Menten, A. M. Koekemoer, E. Kreysa, P. Kurczynski, H. W. Rix, E. Schinnerer, and P. P. Van Der Werf. The large apex bolometer camera survey of the extended Chandra deep field south. *Astrophys. J.*, 707(2):1201–1216, 2009.

A. Weiß, C. De Breuck, D. P. Marrone, J. D. Vieira, J. E. Aguirre, K. A. Aird, M. Aravena, M. L. Ashby, M. Bayliss, B. A. Benson, M. Béthermin, A. D. Biggs, L. E. Bleem, J. J. Bock, M. Bothwell, C. M. Bradford, M. Brodwin, J. E. Carlstrom, C. L. Chang, S. C. Chapman, T. M. Crawford, A. T. Crites, T. De Haan, M. A. Dobbs, T. P. Downes, C. D. Fassnacht, E. M. George, M. D. Gladders, A. H. Gonzalez, T. R. Greve, N. W. Halverson, Y. D. Hezaveh, F. W. High, G. P. Holder, W. L. Holzapfel, S. Hoover, J. D. Hrubes, K. Husband, R. Keisler, A. T. Lee, E. M. Leitch, M. Lueker, D. Luong-Van, M. Malkan, V. McIntyre, J. J. McMahon, J. Mehl, K. M. Menten, S. S. Meyer, E. J. Murphy, S. Padin, T. Plagge, C. L. Reichardt, A. Rest, M. Rosenman, J. Ruel, J. E. Ruhl, K. K. Schaffer, E. Shirokoff, J. S. Spilker, B. Stalder, Z. Staniszewski, A. A. Stark, K. Story, K. Vanderlinde, N. Welikala, and R. Williamson. Alma redshifts of

doi:10.6342/NTU201800137

millimeter-selected galaxies from the SPT survey: The redshift distribution of dusty star-forming galaxies. *Astrophys. J.*, 767(1), 2013.

S. D. M. White and M. J. Rees. Core condensation in heavy halos: a two-stage theory for galaxy formation and clustering. *Mon. Not. R. Astron. Soc.*, 183(3):341–358, 1978.

A. Wilkinson, O. Almaini, C. C. Chen, I. Smail, V. Arumugam, A. Blain, E. L. Chapin, S. C. Chapman, C. J. Conselice, W. I. Cowley, J. S. Dunlop, D. Farrah, J. Geach, W. G. Hartley, R. J. Ivison, D. T. Maltby, M. J. Michalowski, A. Mortlock, D. Scott, C. Simpson, J. M. Simpson, P. van der Werf, and V. Wild. The SCUBA-2 Cosmology Legacy Survey: The clustering of submillimetre galaxies in the UKIDSS UDS field. *Mon. Not. R. Astron. Soc.*, 464(2):1380–1392, 2017.

C. C. Williams, M. Giavalisco, C. Porciani, M. S. Yun, A. Pope, K. S. Scott, J. E. Austermann, I. Aretxaga, B. Hatsukade, K. S. Lee, G. W. Wilson, R. Cybulski, D. H. Hughes, R. Kawabe, K. Kohno, T. Perera, and F. P. Schloerb. On the clustering of submillimeter galaxies. *Astrophys. J.*, 733(2), 2011.

J. Q. Xia, M. Negrello, A. Lapi, G. De Zotti, L. Danese, and M. Viel. Clustering of submillimetre galaxies in a self-regulated baryon collapse model. *Mon. Not. R. Astron. Soc.*, 422(2):1324–1331, 2012.

I. Zehavi, Z. Zheng, D. H. Weinberg, M. R. Blanton, N. A. Bahcall, A. A. Berlind, J. Brinkmann, J. A. Frieman, J. E. Gunn, R. H. Lupton, R. C. Nichol, W. J. Percival, D. P. Schneider, R. A. Skibba, M. A. Strauss, M. Tegmark, and D. G. York. Galaxy clustering in the completed sdss redshift survey: The dependence on color and luminosity. *Astrophys. J.*, 736(1), 2011.

doi:10.6342/NTU201800137